

## Predicting reproductive phenology of wind-pollinated trees via PlanetScope time series

Yiluan Song <sup>a,b,c,\*,</sup>, Daniel S.W. Katz <sup>d</sup>, Zhe Zhu <sup>e</sup>, Claudie Beaulieu <sup>f,</sup>, Kai Zhu <sup>a,b,c,\*</sup>

<sup>a</sup> School for Environment and Sustainability and Institute for Global Change Biology, University of Michigan, Ann Arbor, MI, USA

<sup>b</sup> Michigan Institute for Data and AI in Society, University of Michigan, Ann Arbor, MI, USA

<sup>c</sup> Department of Environmental Studies, University of California, Santa Cruz, CA, USA

<sup>d</sup> School of Integrative Plant Science, Cornell University, Ithaca, NY, USA

<sup>e</sup> Department of Natural Resources and the Environment, University of Connecticut, Storrs, CT, USA

<sup>f</sup> Department of Ocean Sciences, University of California, Santa Cruz, CA, USA



### ARTICLE INFO

#### Keywords:

Airborne pollen  
Flowering phenology  
Time series analysis  
Leaf-out phenology

### ABSTRACT

Airborne pollen triggers allergic reactions, which can have public health consequences. Accurate airborne pollen concentration modeling and prediction rely on understanding plant reproductive phenology, particularly the timing of flowering and pollen release. Flowering and pollen phenology data are often collected through ground observations and air sampling, but such *in-situ* data collection efforts are expensive and spatially sparse. In contrast to *in-situ* data collection, satellite-based estimates of plant phenology could potentially enable large-scale data collection, but it is challenging to detect the reproductive phenology of wind-pollinated flowers from space. Here, we infer the reproductive phenology of wind-pollinated plants on the individual tree level and city level using PlanetScope time series with a spatial resolution of 3 m and a daily revisit cycle. We complemented PlanetScope data by *in-situ* flower and pollen observations at the two scales, leveraging the correlation between vegetative and reproductive phenology. On the individual tree level, we extracted PlanetScope-derived green-up time and validated its correlation to flowering time using flower observations in a national-scale observatory network. Scaling up to the city level, we developed a novel approach to characterize pollen phenology from PlanetScope-derived vegetative phenology, by optimizing two tuning parameters: the threshold of green-up or green-down and the time lag between green-up/down and flowering. We applied this method to seven cities in the US and 14 key wind-pollinated tree genera, calibrated by measurements of airborne pollen concentrations. Our method characterized pollen phenology accurately, not only in-sample (Spearman correlation: 0.751, nRMSE: 13.5 % for *Quercus* spp.) but also out-of-sample (Spearman correlation: 0.691, nRMSE: 14.5 % for *Quercus* spp.). Using the calibrated model, we further mapped the pollen phenology landscape within cities, showing intra-urban heterogeneity. Using high spatiotemporal resolution remote sensing, our novel approach enables us to infer the flowering and pollen phenology of wind-pollinated plant taxa on a large scale and a fine resolution, including areas with limited prior *in-situ* flower and pollen observations. The use of PlanetScope time series therefore holds promise for developing process-based pollen models and targeted public health strategies to mitigate the impact of allergenic pollen exposure.

### 1. Introduction

Pollen is a trigger of allergic asthma and allergic rhinitis (hay fever), imposing significant costs on public health (Reid and Gamble, 2009; D'Amato et al., 2020; Idroso et al., 2022; A. B. Singh & Kumar, 2022). The onset, duration, and intensity of pollen seasons are highly related to

the phenology, the timing of recurring biological events, of wind-pollinated plants. Health risks from pollen exposure are likely to exacerbate under global change, reflected in earlier starts and often longer durations of flowering seasons (Mo et al., 2017) and pollen seasons (Anderegg et al., 2021; Ziska et al., 2011, 2019), as well as higher pollen concentrations (Ziska and Caulfield, 2000). Currently, the

\* Corresponding author. School for Environment and Sustainability and Institute for Global Change Biology, University of Michigan, Ann Arbor, MI, USA.

\*\* Corresponding author. School for Environment and Sustainability and Institute for Global Change Biology, University of Michigan, Ann Arbor, MI, USA.

E-mail addresses: [songyl@umich.edu](mailto:songyl@umich.edu) (Y. Song), [zhukai@umich.edu](mailto:zhukai@umich.edu) (K. Zhu).

sparsity of pollen concentration data and the lack of operational process-based ('numerical') pollen models (D. Katz et al., 2024), especially outside of Europe and Australia, hinder accurate assessments and timely public health responses to changing pollen seasons exacerbated by global changes. The elevating risks call for major improvements in the collection of flower and pollen phenology data on large scales and fine resolutions, in order to enhance mechanistic understanding and prediction of the reproductive phenology of wind-pollinated plants.

Previous research on plant reproductive phenology for public health has been limited by insufficient observational data. In the field of aerobiology, pollen phenology is studied with airborne pollen concentration data from air sampling, generally through national pollen monitoring networks (Scheifinger et al., 2013). These pollen concentration data are collected with systematic protocols, serving as a high-quality source for pollen modeling. However, air sampling of pollen is expensive, and the stations are temporally and spatially sparse (Anderegg et al., 2021). Aggregated over a large area and identified to the family or genus level, pollen samples often do not allow us to study fine-scale spatial variations and intra-genus variations. An exception is pollen monitoring in Europe, where pollen concentration data are often processed bi-hourly in Europe (Galán et al., 2014) and soon to be generated by automated instruments in real time (Immler and Tziastas, 2024). In the field of ecology, ground observations of flowering phenology, from observatory networks and community science, have been correlated with pollen phenology (Crimmins et al., 2017; Elmedorf et al., 2016; Templ et al., 2018). These phenological observations have a larger spatial coverage and a finer taxonomic resolution compared to air sampling data but are limited by subjectivity in the classification of phenophases (Donnelly et al., 2022) and spatiotemporal sampling bias (Pearse et al., 2017).

Although both air samples and ground observations have been used to advance pollen modeling, these models still need to be improved in accuracy and spatial robustness (Scheifinger et al., 2013; Suanno et al., 2021; Zhu et al., 2024). On the one hand, data-driven pollen models using statistics (Frenguelli et al., 1989) or machine learning (Seo et al., 2019; Zewdie et al., 2019; F. Lo et al., 2021) are usually site-specific and sometimes lack accuracy (Chuine and Belmonte, 2004; Maya-Manzano et al., 2021). It is therefore challenging to extrapolate locally-trained pollen models to locations without prior *in-situ* data collection. Integration of land surface phenology as predictors has been suggested to improve data-driven models (Huete et al., 2019; F. Lo et al., 2021). On the other hand, process-based pollen models that explicitly account for plant reproductive phenology, pollen production, and pollen dispersion have been shown to be promising in predicting pollen seasons with robustness across Europe (Chuine and Belmonte, 2004; Sofiev et al., 2006, 2015, 2024; Vogel et al., 2008; García-Mozo et al., 2009; Mimić et al., 2021; Verstraeten et al., 2022, 2024) and predicting spatial variations of pollen concentrations within cities in the US (D. S. W. Katz et al., 2023). Several gaps exist in the current process-based pollen models outside of Europe: they are rarely updated with near real-time observations; they are not available on an operational scale; they are usually limited in spatial resolution, missing important heterogeneity within cities (Katz and Batterman, 2020). To create generalizable and granular process-guided models of airborne pollen, we need to go beyond existing empirical data and obtain plant reproductive phenology data with a large spatial coverage and fine spatial resolution.

To overcome the data challenge, remote sensing has been explored to inform pollen and flower phenology, building on the correlation between reproductive phenology and vegetative phenology. Leaf out and flowering, are tightly linked phenological events in a plant's life cycle, evolved to occur in a predictable sequence with stable time intervals (Davies et al., 2013; Guo et al., 2023). Such flower-leaf sequences are crucial to plant fitness in temperate regions (Buonaiuto and Wolkovich, 2021; Guo et al., 2023), such as through effective wind pollination in flowering-first species (Buonaiuto et al., 2021). Such a biophysical relationship motivates the inference of reproductive phenology from

remotely-sensed vegetative phenology (Davies et al., 2013). For example, the onset of bud burst detected from Moderate Resolution Imaging Spectroradiometer (MODIS) Normalized Difference Vegetation Index (NDVI) and Global Inventory Monitoring and Modeling System (GIMMS) NDVI were found to correlate with the onset of birch flowering (Karlsen et al., 2008) and birch pollen season (Högda et al., 2002), respectively, on continental and decadal scales. Interannual variations in the flowering time of multiple plant functional types have been explained by remotely sensed green-up time (Delbart et al., 2015). Moving beyond correlation, data-driven predictive pollen models have also benefited from incorporating MODIS Enhanced Vegetation Index (EVI) as a predictor (Huete et al., 2019; F. A. Lo, 2020; Yang et al., 2022). These studies show the feasibility of using satellite remote sensing to greatly expand the spatial coverage of reproductive phenology data and to improve pollen models.

Despite their broad spatial coverage, satellite remote sensing data products previously used to study flowering and pollen phenology have a limited spatial resolution, specifically 250 m (MODIS), 500 m (MODIS), or 8 km (GIMMS). Land surface phenology detected on this resolution suffers from the mixed pixel problem (X. Chen et al., 2018). This is particularly problematic for urban landscapes that are highly heterogeneous in land cover and plant species. Given that pollen exposure and plant reproductive phenology are highly spatially heterogeneous within a city (D. S. W. Katz et al., 2019; D. S. W. Katz and Carey, 2014), land surface phenology at a coarse spatial resolution does not satisfy the need for spatially-explicit pollen modeling for public health.

With a spatial resolution of 3 m and a daily revisit cycle, PlanetScope data provide an excellent opportunity to gather plant reproductive phenology data on a large scale and at an individual tree level. We identified the untapped potential of PlanetScope data for public health from two streams of research. On the one hand, PlanetScope data have been used to successfully detect large and brightly-colored flowers within a stand, with indices designed to capture spectral signatures of flowers, such as enhanced bloom index (EBI) (Campbell and Fearn, 2018; B. Chen et al., 2019; Dixon et al., 2021). Although supporting the use of PlanetScope to detect canopy-level phenological variations, the PlanetScope-derived bloom index can hardly be applied to wind-pollinated flowers that are small and inconspicuous (Kim et al., 2020). Reproductive phenology of wind-pollinated flowers will therefore largely rely on the inference from vegetative phenology. On the other hand, PlanetScope-derived EVI has been shown to be a reliable data source for tree-level vegetative phenology, validated by other remote sensing data products (Moon et al., 2021) and ground observations (Moon et al., 2022; Zhao et al., 2022; Y. Liu et al., 2024). Despite promising applications of PlanetScope data to detect spatial variations among individual tree canopies and to derive vegetative phenology, it has not yet been used to infer tree-level flowering phenology from vegetative phenology. Further, to our knowledge, there has not been research linking PlanetScope directly to pollen phenology, which is central to modeling pollen exposure.

In this study, we assessed the potential of using vegetative phenology data extracted from PlanetScope to infer the flowering and pollen phenology of wind-pollinated trees. Specifically, the study focused on answering the following research questions at two scales (Fig. 1, Fig. S1).

**Q1:** On the tree level, does PlanetScope-derived vegetative phenology correlate with flowering phenology monitored by field observations?

**Q2:** Upscaled from the tree level to the city level, can PlanetScope-derived vegetative phenology be used to accurately infer pollen phenology characterized by airborne pollen concentrations? In particular, does this inference extrapolate over a large spatial scale, to locations where airborne pollen concentration data are unavailable?

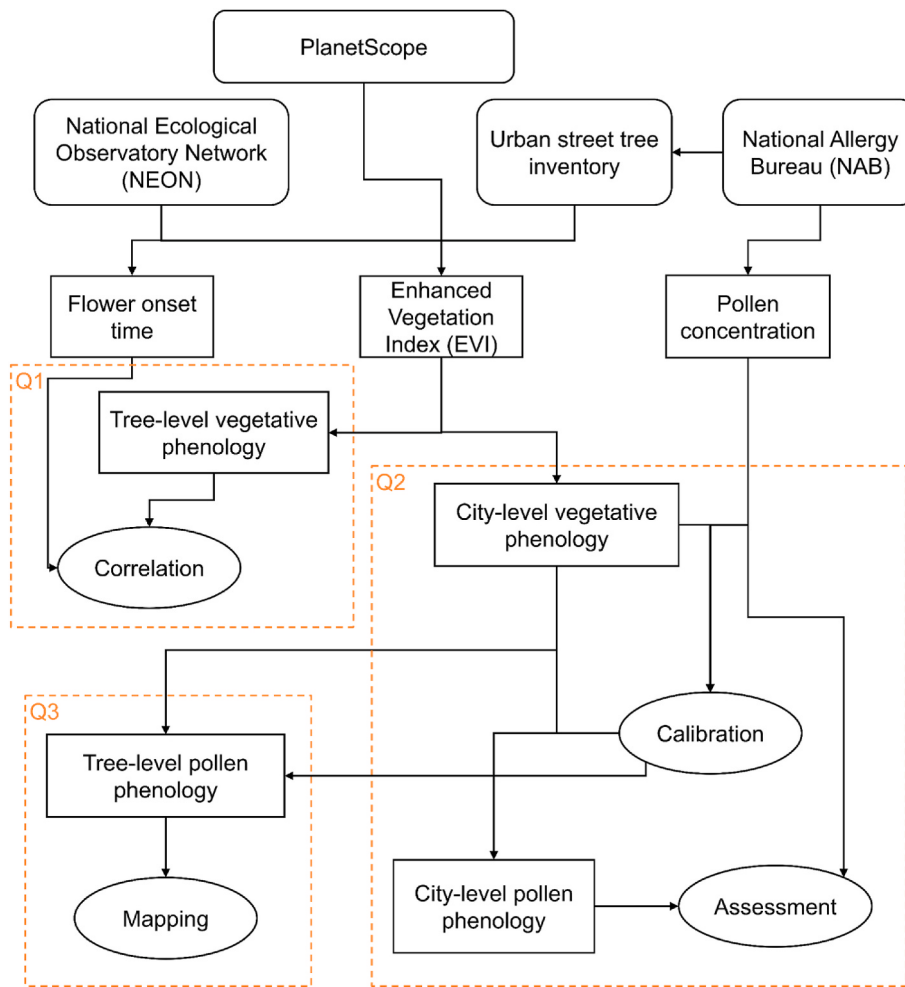


**Fig. 1.** Simplified flow diagram of data and methods used in this study, and corresponding research questions. Rounded rectangles represent source datasets. Rectangles represent derived variables to analyze. Ellipses represent data analysis steps.

**Q3:** Scaling back to the tree level, can PlanetScope-derived vegetative phenology be used to explore fine-scale intra-urban heterogeneity of pollen phenology, i.e., a pollen allergy landscape?

In answering these three questions, we developed a novel workflow for obtaining cross-scale reproductive phenology data from PlanetScope time series. Our workflow has two core ideas: upscaling tree-level green-up/down time to the city-level green-up/down phenology, and tuning two parameters to calibrate city-level green-up/down phenology with city-level *in-situ* pollen phenology.

## 2. Materials and methods

### 2.1. Data description

#### 2.1.1. Tree-level flowering observations

To test whether PlanetScope can capture tree-level variations in flowering phenology, we retrieved plant phenology observations from the National Ecological Observatory Network (NEON) (DP1.10055.001) that were integrated into the USA National Phenology Network (USA-NPN) (Elmendorf et al., 2016; Crimmins et al., 2017; National Ecological Observatory Network, 2020). At each site and every year, 90–100 tagged individual plants were observed *in situ* by trained technicians for their vegetative and reproductive phenophase status with varying sampling frequencies up to three times per week, following the phenophase definitions and protocols of NPN (Denny et al., 2014). We downloaded individual phenometrics from the NEON data submitted to

NPN, which are the estimates of the dates of phenophase onsets and ends, measured from a series of consecutive "yes" phenophase status records. In this study, we used flower and leaf onset dates, which are the time of first "yes" observations for an individual tree in a given year. To complement the phenological data, we retrieved the accurate coordinates of tagged NEON trees using the R package *geoNEON* (National Ecological Observatory Network, 2023). We focused on primary sampling sites within the conterminous United States that have available coordinates of tagged individual plants (Fig. S2). We included data from 2018 to 2022, as fully operational PlanetScope data collection started in 2018 (Fig. S3).

We focused on 14 deciduous wind-pollinated tree species with considerable public health impacts and high abundance in the conterminous United States (Crimmins et al., 2023; F. Lo et al., 2019): *Acer* spp. (maple), *Alnus* spp. (alder), *Betula* spp. (birch), *Carya* spp. (hickory), *Celtis* spp. (hackberry), *Fraxinus* spp. (ash), *Juglans* spp. (walnut), *Liquidambar* spp. (sweetgum), *Morus* spp. (mulberry), *Platanus* spp. (plane, sycamore), *Populus* spp. (poplar, aspen, cottonwood), *Quercus* spp. (oak), *Salix* spp. (willow), and *Ulmus* spp. (elm). *Ulmus* spp. were considered to have an early- and a late-flowering group, whose phenology was analyzed separately.

#### 2.1.2. City-level pollen concentration from air sampling and street-tree inventory

To examine the potential of using PlanetScope for city-level pollen phenology and to inform public health, we obtained consistent and accurate pollen concentration data from stations associated with the

American Academy of Allergy, Asthma & Immunology (AAAAI) National Allergy Bureau (NAB) (AAAAI, 2022) (Figs. 2 and 3). At around 80 stations located throughout the conterminous US, airborne pollen was sampled daily using volumetric impactor samplers (mostly Burkard samplers and sometimes Rotorod samplers) (Portnoy et al., 2004; M. Bastl et al., 2023; Levetin et al., 2023), and then classified to the genus or family level and counted by NAB-certified operators. Despite possible differences in absolute pollen concentration estimated using Burkard and Rotorod samplers, these two methods are consistent in quantifying the seasonal trends of pollen of the same taxa (Frenz, 1999; Crisp et al., 2013; Crimmins et al., 2023), allowing us to study taxa-specific pollen phenology. The NAB dataset is the most commonly used data source for the description and prediction of pollen phenology in public health and ecological research in North America. We obtained pollen concentration data collected from 2003 until late 2023 (Fig. 3). Data were available during most springs and summers after the establishment of sampling stations, with missing data when airborne concentrations were low (Fig. S4). As in the tree-level analysis, we focused on the pollen phenology of 14 wind-pollinated tree genera (*Acer*, *Alnus*, *Betula*, *Carya*, *Celtis*, *Fraxinus*, *Juglans*, *Liquidambar*, *Morus*, *Platanus*, *Populus*, *Quercus*, *Salix*, and *Ulmus*).

To complement the pollen concentration data, we obtained street tree inventories in selected cities (Figs. 2 and 4; details on sources of tree inventories in Table S1). Necessary reprojections were performed to convert all coordinates in street tree inventories to longitude and latitude. The taxonomy of street trees was resolved with the R package *taxize* (Chamberlain and Szöcs, 2013) for selecting trees in the genus of interest. When there were more than 2000 recorded trees of a genus in a city, we randomly selected 2000 trees (Psutka and Psutka, 2019).

We focused on seven US cities with an available street tree inventory and a nearby pollen monitoring station (Fig. 2): Austin (AT), Detroit (DT), Denver (DV), Houston (HT), New York (NY), Seattle (ST), and Tampa (TP). Most focal cities have a pollen monitoring station within the city, with a mean distance from the pollen monitoring station to the centroid of all censused street trees ranging from 3.7 km to 41 km. This is well within the footprint of a volumetric pollen monitoring station, which can cover a region within a radius of about 100 km (M. Bastl et al., 2023). Two exceptions were that Denver's pollen concentration data

were from Colorado Springs (mean distance 97 km) and that Detroit's pollen concentration data were from Sylvania (mean distance 91 km). Of the seven stations, most were confirmed to use Burkard samplers, except that Colorado Springs might have used a Rotorod sampler.

As an additional data source for validation, we retrieved flower and pollen cone observations from the USA National Phenology Network (NPN) dataset (Rosemartin et al., 2018). Data were contributed by volunteers through the Nature's Notebook mobile app. We downloaded phenophase status observations of the 14 genera of interest from 2000 to 2024. We focused on observations for the following phenophases relevant to plant reproduction: "Full pollen release (conifers)", "Pollen release (conifers)", "Pollen cones (conifers)", "Open pollen cones (conifers)", "Full flowering (50 %)", "Flowers or flower buds", and "Pollen release (flowers)." We kept observations within a 500 km radius of each of the seven NAB stations of interest in order to include sufficient data points that are relevant to local pollen concentration. For each taxon, site, and date, we calculated the percentage of "Yes" observations for the above phenophases out of all "Yes" and "No" observations (Crimmins et al., 2023). This percentage between 0 % and 100 % is a proxy for the reproductive status of plants in an area (Fig. S5) that could later be used to compare with inferred pollen phenology.

### 2.1.3. PlanetScope reflectances for vegetative phenology

We retrieved PlanetScope images from 2017 to 2023 for all trees involved in the analyses, including sampled trees at NEON sites and street trees from 14 wind-pollinated tree genera in seven selected US cities (Fig. 4). We downloaded the PlanetScope atmospherically corrected surface reflectance product (ortho\_analytic\_4b\_sr) (Planet Team, 2017) through the Planet API, using a custom package based on the R package *planetR* (Bevington et al., 2024). We applied the "harmonize" tool in the Planet API with "Sentinel-2" as the target sensor, in order to make all PlanetScope data consistent and approximately comparable to Sentinel-2 data (Kington and Collison, 2022). All images obtained were acquired during the day (sun elevation >0 m). At the coordinates of the trees of interest, we obtained the reflectances in the red, green, blue, and near-infrared bands. For quality control, we applied Useable Data Masks (UDM2) (Planet Team, 2023) to include only pixels that were clear, had no snow, ice, shadow, haze, or cloud, and had algorithmic confidence in

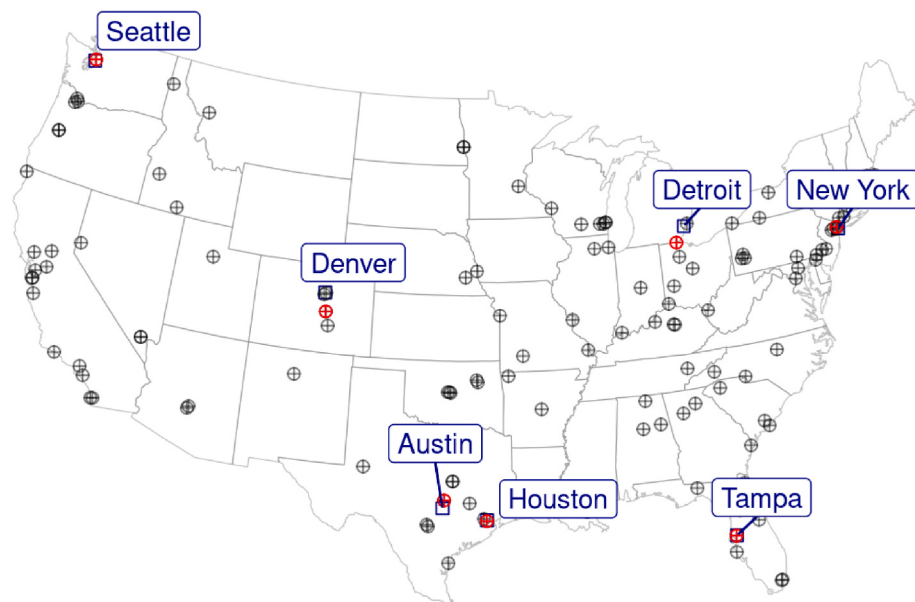


**Fig. 2.** Map of seven studied cities with street tree inventory (blue squares) and pollen monitoring stations associated with the National Allergy Bureau (NAB) (red crossed circles). Street tree inventory was used to locate known wind-pollinated trees and to extract their phenological signals from remote sensing. Pollen monitoring stations provide pollen concentration data for calibration and validation of the model that predicts pollen phenology with remote sensing data. Pollen monitoring stations were located within 100 km of the centroid of the city's street trees. Other NAB pollen monitoring stations not used in this analysis are marked in gray crossed circles.

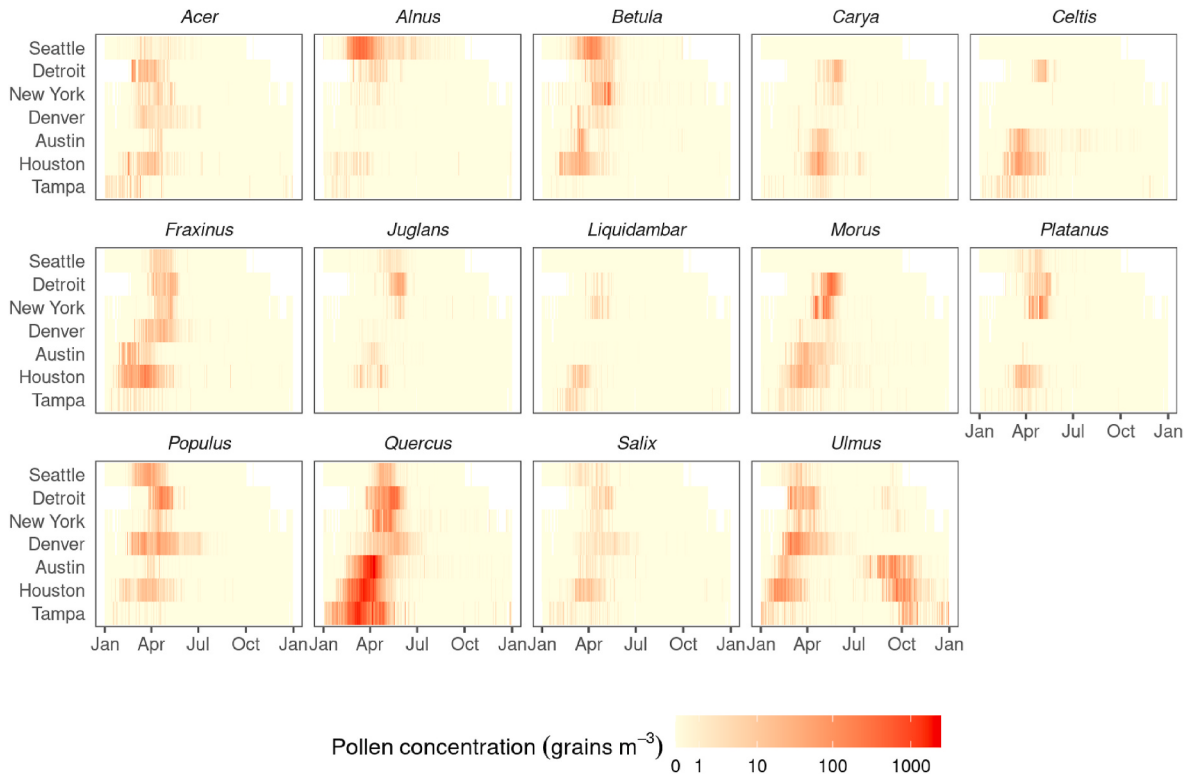


**Fig. 3.** Climatologies of daily pollen concentration ( $\text{grains m}^{-3}$ ) of 14 key pollen-producing genera in studied cities. Climatologies were calculated by averaging the data for the same day of the year across all years over the period 2003–2023. Most genera have pollen peaks in the spring, except for *Ulmus* which have pollen peaks in both the spring and fall. Cities are ordered according to their latitude, showing latitudinal trends in the time of pollen peak. Data are from the National Allergy Bureau (NAB) pollen monitoring stations.

classification  $\geq 80\%$ . Given little information on the size and shape of trees, we obtained reflectances at the focal coordinates, instead of within polygons that cover tree canopies (Dixon et al., 2023). For each date, pixel, and band, we computed mean reflectances if there were multiple visits in a day.

## 2.2. Data processing

### 2.2.1. Curating ground-observed flowering phenology data

In processing the NEON flowering phenology data, we exclude NEON sites located outside the conterminous United States. We also excluded sites situated in the Mediterranean climatic zone (all sites in California), where plant phenology is primarily driven by precipitation instead of temperature, distinct from other parts of the conterminous US. We focused on wind-pollinated tree species that were widely represented in the NEON data ( $\geq 50$  records). We removed outliers of spring flower onset dates that were biologically implausible for the species present in the dataset (later than day 150).

### 2.2.2. Curating air-sampled pollen concentration data

We processed NAB pollen concentration data to characterize pollen phenology in several steps.

- 1) In order to include at least one full pollen peak, we extended data in each year in both directions, into day-of-year (DOY) 275 (Oct 2) in the previous calendar year and into day 90 (Mar 30) in the following calendar year. Data on day 366 in leap years were ignored. This extended duration covers a total of 546 days.
- 2) We removed combinations of genus and city when there were no trees of interest in the street tree inventory, or there were no more than 30 pollen concentration records greater than or equal to  $0 \text{ grains m}^{-3}$ . We removed *Fraxinus* spp. from New York and Detroit

from our dataset due to the mass die-off of these two trees in these two cities during our study period.

- 3) To compress extreme values and stabilize the variance, we transformed all pollen concentration values  $[\text{pollen}]_{gcT}(t)$  to their square root  $\sqrt{[\text{pollen}]_{gcT}(t)}$  (K. Bastl et al., 2018; Bonini et al., 2022). Here,  $t$  represents the day of year. Indices  $g$ ,  $c$ ,  $T$  represent genus, city, and year, respectively.
- 4) In order to focus on single pollen peaks for plant genera that have both early- and late-flowering variations (e.g., *Ulmus* spp.), as well as to reduce the confounding effect of outliers outside the reproductive season, we constrained the pollen seasons for each taxon, setting the pollen concentration outside the season to zero. Genus-specific pollen seasons were determined by summing the total pollen concentration over all cities and years, fitting a Gaussian kernel, calculating a window of mean  $\pm 1.96 \times$  standard deviation (Zhang and Steiner, 2022), and extending the window by 50 days on both ends (Fig. S6). An exception was that the early and late pollen windows of *Ulmus* spp. were detected by fitting a Gaussian mixture model with two peaks.

To handle short gaps of missing data within the pollen peaks and reduce the impacts of outliers, we gap-filled and smoothed the time series with weighted Whittaker smoothing  $S(\sqrt{[\text{pollen}]_{gcT}(t)})$  (Eilers, 2003, 2004). Here  $S$  refers to a weighted Whittaker smoothing operation.

### 2.2.3. Calculating enhanced vegetative index from PlanetScope reflectances

In order to characterize tree-level vegetative phenology, we used reflectances from PlanetScope images to extract phenological metrics, specifically green-up or green-down time, for each individual tree of interest. We performed the following steps.



**Fig. 4.** A subset of street trees in Detroit overlaid on a true-color PlanetScope image on May 8, 2017. The extent of the area is 83.1630°W to 83.1381°W longitude and 42.3869°N to 42.4054°N latitude. The true-color image was constructed with the reflectances in the red, green, and blue bands, with brightness adjusted. The colors of points indicate street trees of different genera. Note that as we show only a small part of Detroit, the genera here do not represent all allergenic genera present in Detroit.

- 1) We calculated the enhanced vegetation index (EVI) (H. Q. Liu and Huete, 1995) (Eqn. (1)). PlanetScope EVI has been shown to accurately extract leaf phenology metrics validated by local digital camera imagery (PhenoCams), robust to different atmospheric conditions and less likely to saturate in densely vegetated areas compared to PlanetScope normalized difference vegetation index (NDVI) (Wu et al., 2021).

$$\text{EVI} = \frac{2.5 \times (\text{NIR} - \text{Red})}{\text{NIR} + 6 \times \text{Red} - 7.5 \times \text{Blue} + 1} \quad (\text{Equation 1})$$

We used the following criteria to filter out possibly erroneous EVI values: reflectances in all visible bands were positive values, and EVI was between zero and one.

- 2) We extended the time series in each year from day 275 (Oct 2) in the previous calendar year to day 90 (Mar 30) in the following year (spanning 546 days) in order to include at least one full growing season with green-up and green-down. This step was necessary for the detection of green-up day when EVI increases from the minimum before the New Year, and the detection of green-down day when EVI decreases to the minimum after the New Year. We gap-filled and smoothed all extended time series  $S(\text{EVI}(t))$  with weighted Whittaker smoothing  $S(\text{EVI}(t))$  (Kong et al., 2019).
- 3) We selected a time series of EVI with significant seasonality. In particular, we fitted a simple linear regression model and then three piecewise regression models with one, two, and three change points, respectively (Eqn. (2)) (Beaulieu and Killick, 2018).

$$\text{Model 1 : } S(\text{EVI}(t)) = \lambda + \beta t + \varepsilon_t$$

Model 2,3,4 take the following form with  $m = 1, 2, 3$  respectively:

$$S(\text{EVI}(t)) = \begin{cases} \lambda_1 + \beta_1 t + \varepsilon_t, & t \leq c_1 \\ \lambda_2 + \beta_2 t + \varepsilon_t, & c_1 < t \leq c_2 \\ \vdots & \vdots \\ \lambda_{m+1} + \beta_{m+1} t + \varepsilon_t, & c_m < t \end{cases} \quad (\text{Equation 2})$$

EVI time series from each genus, city, year, and tree were analyzed separately, but we omit the indices here for simplicity. In Model 1,  $t$  represents the time in days,  $\lambda$  and  $\beta$  represent the intercept and trend and  $\varepsilon_t$  is white noise. In Models 2–4,  $m$  represents the number of changepoints,  $c_m$  ( $m = 1, \dots, 3$ ) represent the timing of change points, and  $\lambda_1, \dots, \lambda_m$  and  $\beta_1, \dots, \beta_m$  represent the intercept and trend in each segment. Piecewise regression models were fitted with R package *segmented* (Muggeo, 2008). We ranked the four models according to the Akaike information criterion (AIC). If a simple linear regression was the best model, we discarded the time series as it may lack seasonal changes in greenness.

### 2.3. Inferring reproductive phenology with PlanetScope

#### 2.3.1. Inferring flowering phenology on the tree level

For individual trees at NEON sites (Fig. S1) monitored for phenology, we used the EVI time series to identify the green-up phases empirically (Fig. 5). The end of a green-up phase (usually in the summer) was determined as the day of year when EVI reaches the maximum in the growing season. The start of a green-up phase (usually in the winter) was then determined as the day of year when EVI is at the minimum, prior to the end of the green-up phase. We then determined the timing of green-up at the 50 % threshold (usually in the spring). This empirical method of defining green-up/down time has been widely applied to remote-sensing data in order to be compatible with different plant functional types with various seasonality that exhibit intra-annual changes in greenness (Moon et al., 2021). We tested the correlation between the 50 % green-up time and the flowering time measured by the day of flower onset in the corresponding year from 2018 to 2022. We assessed the

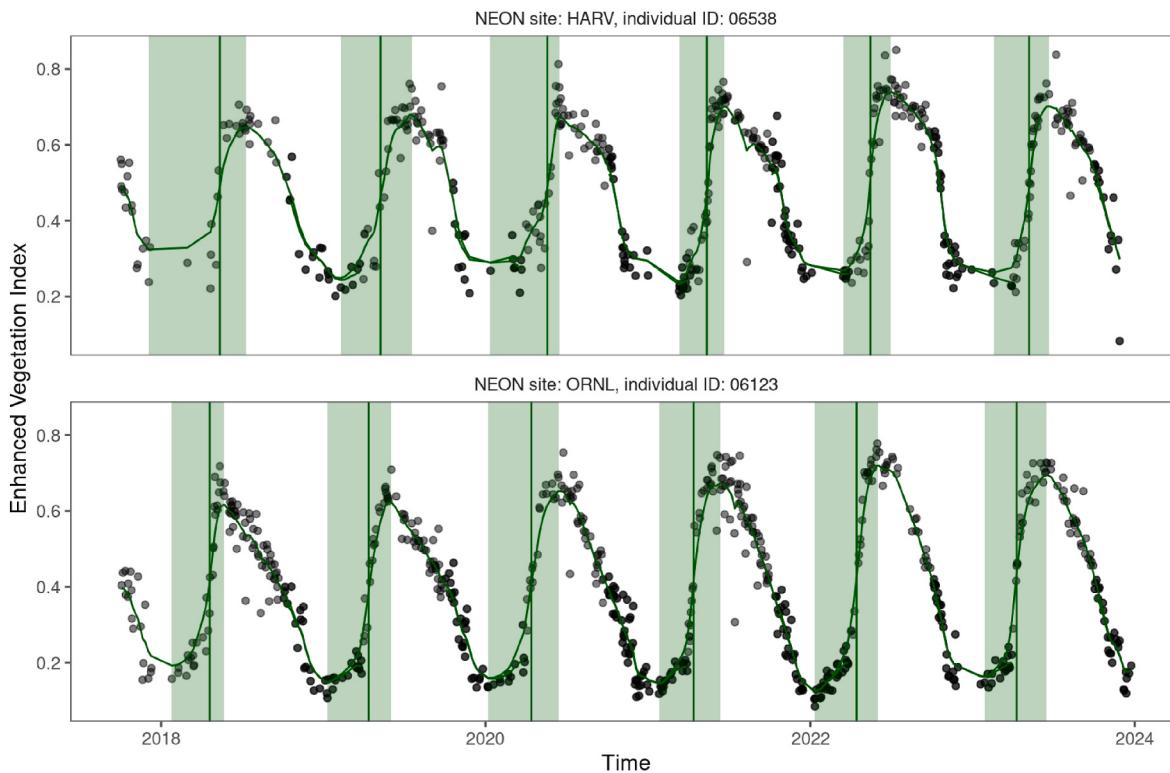


**Fig. 5.** Extraction of tree-level phenological metric from PlanetScope data for wind-pollinated trees sampled at the National Ecological Observatory Network (NEON). We show two trees at Harvard Forest & Quabbin Watershed (HARV, 42.53691° N, 72.17265° W) and Oak Ridge (ORNL, 35.96413° N 84.28259° W) sites as examples. Black points are Enhanced Vegetation Index (EVI) calculated from PlanetScope reflectances at the coordinates of the trees of interest. Green lines are smoothed EVI. Green shades indicate the period of green-up extracted from smoothed EVI curves, spanning the time with minimum EVI in the winter and the time with maximum EVI in the summer in each growing season. Vertical green lines are 50 % green-up time in each growing season, which is the time when EVI crosses 50 % of the range between minimum EVI and maximum EVI.

Pearson correlation coefficients and the significance of the correlations across all sites.

### 2.3.2. Inferring pollen phenology on the city level

To infer city-level pollen phenology from tree-level vegetative phenology monitored by PlanetScope, we developed the following nonparametric algorithm with two tuning parameters (Fig. 6, Algorithm

1, Eqns. (3)–(7)). We first extracted the timing of green-up/down events for individual trees at various thresholds based on their EVI curves. These individual events were then upscaled to city-level vegetative phenology. Next, we applied various time lags to vegetative phenology to derive city-level pollen phenology. Finally, we optimized thresholds and lags with air-sampled city-level pollen phenology. We describe the details of the algorithm below.

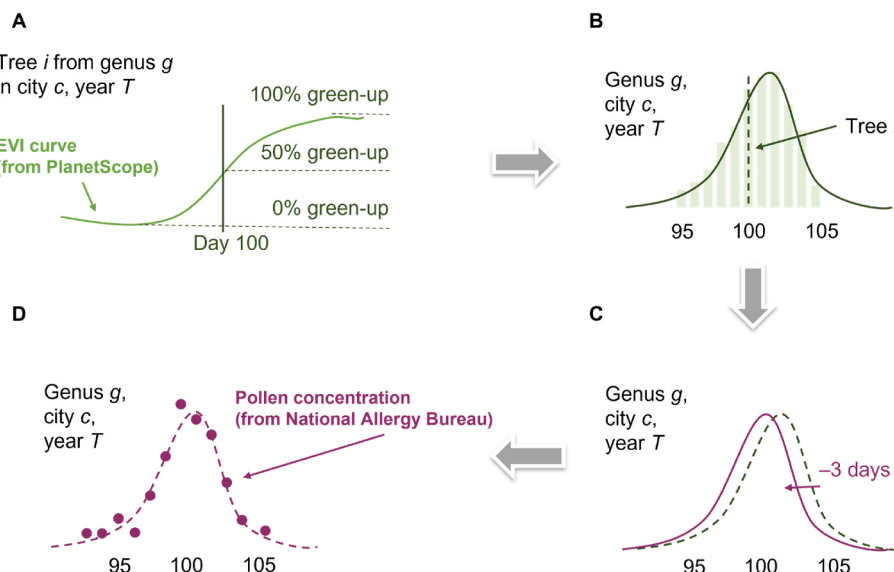


**Fig. 6.** Nonparametric algorithm for inferring pollen phenology from vegetative phenology derived from PlanetScope. The model has four main steps: (A) Extract tree-level green-up/down date at threshold  $\theta_g$  (e.g.,  $\theta_g = 50\%$ ). (B) Upscale to city-level leaf phenology. (C) Shift to city-level pollen phenology with leaf-pollen lag  $\delta_{gc}$  (e.g.,  $\delta_{gc} = -3$  days). (D) Compare with city-level pollen concentration.

1) We first extracted the timing of green-up/down for all trees of interest as the day of year when their growing season EVI curves first cross the green-up/down threshold  $\theta_g$  (Eqn. (3)). We used a similar algorithm to that described in section 2.3.1 (Fig. 5). The end of a green-up phase (usually in the summer) was determined as the day of year when EVI reaches the maximum in the growing season. The start of a green-up phase was then determined as the day of year when EVI is at the minimum (usually in the previous winter), prior to the end of the green-up phase. Similarly, the start of a green-down phase (usually in the summer) was determined as the day of year when EVI reaches the maximum in the growing season; the end of a green-down phase (usually in the following winter) was then determined as the day of year when EVI is at the minimum, after the start of the green-down phase. We then determined the timing of green-up/down at multiple thresholds, including 30 %, 40 %, 50 %, 60 %, and 70 % green-up for genera that flower in the spring (all except late-flowering *Ulmus* spp.), and 70 %, ..., 30 % green-down for late-flowering *Ulmus* spp.

$$\begin{aligned} t_{\text{green-up}}(\theta_g) &= \min\{t \mid \text{EVI}(t) \geq \theta_g(\max_t(\text{EVI}(t)) - \min_t(\text{EVI}(t)))\} \\ t_{\text{peak}} &= \min\{t \mid \text{EVI}(t) \geq \max_t(\text{EVI}(t))\} \\ t_{\text{green-down}}(\theta_g) &= \min \left\{ \begin{array}{l} t \mid t \geq t_{\text{peak}} \text{ and} \\ \text{EVI}(t) \leq \theta_g(\max_t(\text{EVI}(t)) - \min_t(\text{EVI}(t))) \end{array} \right\} \\ \theta_g &\in \{30\%, 40\%, 50\%, 60\%, 70\%\} \end{aligned} \quad (\text{Equation } 3)$$

#### Algorithm 1. Algorithm for inferring city-level pollen phenology from tree-level vegetative phenology.

---

```

1: Input: tree-level EVI curves, city-level pollen phenology
2: Parameters:  $\theta_g$  (green-up/down threshold),  $\delta_{gc}$  (leaf-pollen lag)
3: Step 1: Extract timing of green-up/down
4: for each tree  $i$  in genus  $g$ , city  $c$ , and year  $T$  do
5:   Determine green-up/down timing  $t_{\text{green-up/down}}(\theta_g)$  based on EVI curves and
   green-up/down thresholds  $\theta_g$ .
6: end for
7: Step 2: Upscale to city-level vegetative phenology
8: for each day  $t$  in genus  $g$ , city  $c$ , and year  $T$  do
9:   Calculate frequency of green-up/down events  $\rho_{gcT}(t; \theta_g)$ .
10: end for
11: for each genus  $g$ , city  $c$ , and year  $T$  do
12:   Apply Whittaker smoothing and normalization to  $\rho_{gcT}(t; \theta_g)$  to obtain city-level
   vegetative phenology  $\psi_{gcT}(t; \theta_g)$ .
13: end for
14: Step 3: Shift to city-level pollen phenology
15: for each genus  $g$ , city  $c$ , and year  $T$  do
16:   Shift city-level vegetative phenology  $\psi_{gcT}(t; \theta_g)$  by  $\delta_{gc}$  to obtain city-level
   pollen phenology  $\phi_{gcT}(t; \theta_g, \delta_{gc})$ .
17: end for
18: Step 4: Normalize NAB-derived city-level pollen concentration
19: for each genus  $g$ , city  $c$ , and year  $T$  do
20:   Normalize transformed pollen concentration time series  $\sqrt{[\text{pollen}]_{gcT}(t)}$  before
   and after Whittaker smoothing to obtain NAB-derived city-level pollen phenology
    $\Pi_{gcT}(t)$  and  $\pi_{gcT}(t)$ .
21: end for
22: Step 5: Calibrate tuning parameters
23: for each threshold  $\theta_g$ , genus  $g$ , and city  $c$  do
24:   Perform a grid search to find optimal  $\hat{\delta}_{gc}(\theta_g)$  that minimize total nRMSE
   between  $\phi_{gcT}(t; \theta_g, \delta_{gc})$  and  $\pi_{gcT}(t)$ .
25: end for
26: for each genus  $g$  do
27:   Using  $\hat{\delta}_{gc}(\theta_g)$ , perform a grid search to find optimal  $\hat{\theta}_g$  that minimize total
   nRMSE between  $\phi_{gcT}(t; \theta_g, \hat{\delta}_{gc}(\theta_g))$  and  $\pi_{gcT}(t)$ .
28:   Using  $\hat{\theta}_g$ , find optimal  $\hat{\delta}_{gc}$ .
29: end for
30: Output: Optimized PlanetScope-derived city-level pollen phenology  $\phi_{gcT}(t; \hat{\theta}_g,$ 
 $\hat{\delta}_{gc})$  with best-fit parameters  $\hat{\theta}_g$  and  $\hat{\delta}_{gc}$ .
```

---

Note that the first tuning parameter in our model is  $\theta_g$ , the green-up or green-down threshold in the growing season EVI time series that is used to obtain green-up/down time. We allowed the threshold to vary by genus  $g$ .

2) Given that our pollen concentration data for validation are on the city level rather than tree level, we upscaled the tree-level green-up/down time to the city-level green-up/down frequency  $\rho_{gcT}(t; \theta_g)$  by summarizing the frequency of inferred green-up/down events at green-up/down threshold  $\theta_g$  on day  $t$  in a given genus, city, and year. We then applied a weighted Whittaker smoothing and a normalization such that it sums up to one over all days in a year (Eqn. (4)).

$$\psi_{gcT}(t; \theta_g) = \frac{S(\rho_{gcT}(t; \theta_g))}{\sum_t S(\rho_{gcT}(t; \theta_g))} \quad (\text{Equation } 4)$$

The resulting city-level vegetative phenology  $\psi_{gcT}(t; \theta_g)$  is conceptually similar to a probability density function of observing green-up/down events.

3) Building on the biophysical and empirical relationships between vegetative and reproductive phenology, we assumed that the time of spring pollen emission and the time of leaf-out of a tree has a relatively stable time lag given a specific climate (Buonaiuto and Wolkovich, 2021; Ma et al., 2021; Guo et al., 2023). Late-flowering *Ulmus* spp. is an exception (Woźniak and Steiner, 2017), with little knowledge of the mechanisms of their flowering phenology. We assumed that their flowering time is associated with the senescence phases of vegetative development, similar to other late-flowering species (Rojo et al., 2022). We shifted the city-level vegetative phenology  $\psi_{gcT}(t; \theta_g)$  to the city-level pollen phenology  $\phi_{gcT}(t; \theta_g, \delta_{gc})$  by applying leaf-pollen lags  $\delta_{gc}$  (Eqn. (5)). We allowed leaf-pollen lags to range from -90 days to 90 days ( $\pm 3$  months), at the interval of 1 day. We allowed the lag to vary by both genus and city. We acknowledge that this method simplifies the duration of pollen emission to a single pollen emission date (Dahl et al., 2013), hence only capturing the variations in city-level pollen concentration caused by the variations in pollen emission among trees but not within individual trees.

$$\begin{aligned} \rho_{gcT}(t; \theta_g, \delta_{gc}) &= \psi_{gcT}(t - \delta_{gc}; \theta_g) \\ \delta_{gc} &\in [-90, 90] \cap \mathbb{Z} \end{aligned} \quad (\text{Equation } 5)$$

Note that the second tuning parameter in our model is  $\delta_{gc}$ , which is the time lag between the timing of leaf phenology and pollen phenology.

4) We scaled the air-sampled city-level pollen concentration to one comparable to PlanetScope-derived city-level pollen phenology, providing city-level pollen phenology for calibration and assessment. We performed normalization to transformed pollen concentration time series  $\sqrt{[\text{pollen}]_{gcT}(t)}$  to remove the spatiotemporal differences from local vegetation cover, pollen productivity, and pollen sampling methods. We normalized pollen concentration before and after Whittaker smoothing to obtain NAB-derived city-level pollen phenology  $\Pi_{gcT}(t)$  and  $\pi_{gcT}(t)$  for model assessment and calibration, respectively (Eqn. (6)).

$$\begin{aligned} \Pi_{gcT}(t) &= \frac{\sqrt{[\text{pollen}]_{gcT}(t)}}{\sum_t S(\sqrt{[\text{pollen}]_{gcT}(t)})} \\ \pi_{gcT}(t) &= \frac{S(\sqrt{[\text{pollen}]_{gcT}(t)})}{\sum_t S(\sqrt{[\text{pollen}]_{gcT}(t)})} \end{aligned} \quad (\text{Equation } 6)$$

5) We assume that NAB-derived city-level pollen phenology  $\pi_{gcT}(t)$  matches PlanetScope-derived city-level pollen phenology  $\varphi_{gcT}(t; \hat{\theta}_g, \hat{\delta}_{gc})$  with optimized green-up/down threshold  $\hat{\theta}_g$  and optimized leaf-pollen lag  $\hat{\delta}_{gc}$ . Therefore, we performed a two-step grid search to optimize  $\theta_g$  and  $\delta_{gc}$  based on the normalized root mean square error (nRMSE) between PlanetScope and NAB-derived pollen phenology (Eqn. (7)). Here, we normalized RMSE by the range of NAB-derived city-level pollen phenology  $\pi_{gcT}(t)$  (Jeon et al., 2018; D. Singh and Singh, 2020). We first selected the leaf-pollen lag  $\hat{\delta}_{gc}(\theta_g)$  for each green-up/down threshold  $\theta_g$  that minimized total nRMSE for each genus and city. We then selected the green-up/down threshold  $\hat{\theta}_g$  that minimized total nRMSE for each genus. We used  $\hat{\theta}_g$  to find  $\hat{\delta}_{gc}$  define

$$\text{nRMSE}(x, \tilde{x}) = \sqrt{\frac{1}{N} \sum_{k=1}^N (x_k - \tilde{x}_k)^2} / (\max(x_k) - \min(x_k))$$

Step 1:

$$\hat{\delta}_{gc}(\theta_g) = \arg \min_{\delta_{gc}} \left\{ \sum_T \text{nRMSE}(\pi_{gcT}(t), \varphi_{gcT}(t; \theta_g, \delta_{gc})) \right\}$$

Step 2:

$$\begin{aligned} \hat{\theta}_g &= \arg \min_g \left\{ \sum_c \sum_T \text{nRMSE}(\pi_{gcT}(t), \varphi_{gcT}(t; \theta_g, \hat{\delta}_{gc}(\theta_g))) \right\} \\ \hat{\delta}_{gc} &= \hat{\delta}_{gc}(\hat{\theta}_g) \end{aligned} \quad (\text{Equation 7})$$

Please see Supplementary Note for details on the number of parameters. The PlanetScope-derived vegetative phenology modified by the optimized threshold and lags  $\varphi_{gcT}(t; \hat{\theta}_g, \hat{\delta}_{gc})$  was considered the optimized PlanetScope-derived city-level pollen phenology.

We assessed the accuracy of PlanetScope-derived city-level pollen phenology  $\varphi_{gcT}(t; \hat{\theta}_g, \hat{\delta}_{gc})$  using its Spearman correlation coefficients and nRMSE with NAB-derived city-level pollen phenology  $\Pi_{gcT}(t)$ . Notably, we compared the Spearman correlation coefficients and RMSE for inferring pollen phenology both in-sample and out-of-sample. In-sample tests assessed the ability of the PlanetScope method to characterize variations in pollen phenology, whereas out-of-sample tests assessed the effectiveness of the PlanetScope method to infer pollen phenology for cities with no prior pollen concentration observations. For in-sample tests, all cities were used in the optimization of parameters. For out-of-sample tests, we conducted leave-one-out cross-validation. Specifically, we removed a random city from the training dataset at a time and optimized threshold and lags in the remaining cities. To predict the lag for the city held for validation, we assumed a linear relationship between the lag and the climate of the city (Fig. S7). To avoid overfitting, we used a simple linear relationship with one predictor representing the long-term temperature of each city. Specifically, we used the mean annual temperature in the TerraClimate Climatologies (1981–2010) dataset (Abatzoglou et al., 2018). We used long-term average temperatures from a past period as the method is based on the mechanistic assumption that the leaf-flower relationship is shaped by the long-term climate of the area and remains relatively stable over time (Davies et al., 2013; Guo et al., 2023). With an optimized threshold and a predicted lag, we subsequently inferred pollen phenology from vegetative phenology at the city held for validation. As the out-of-sample tests rely on extrapolation over a climatic gradient, we could only implement them for *Quercus* spp. that were present in all seven cities studied.

In addition to validation with NAB data, we compared the inferred pollen phenology with the percentage of local “Yes” observations of flower and pollen cones from NPN data. As these two variables are on

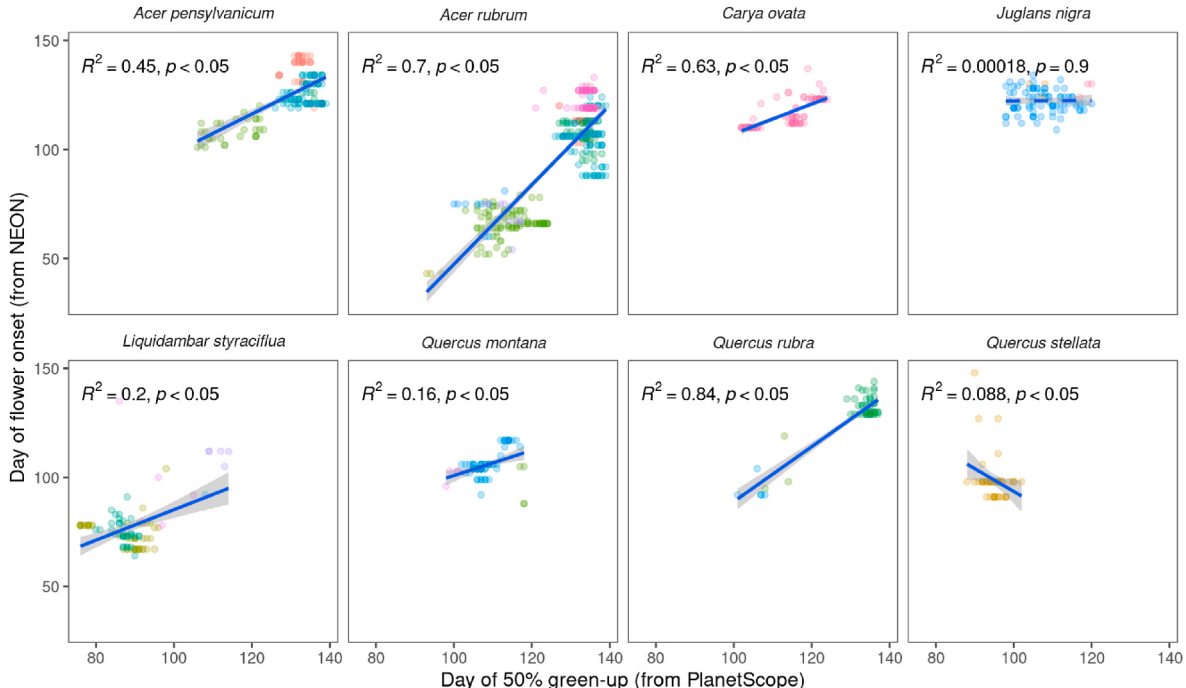


**Fig. 7.** Correlation between 50 % green-up time from PlanetScope and flower onset time from the National Ecological Observatory Network (NEON). 50 % green-up time was calculated as the time when PlanetScope-derived Enhanced Vegetation Index crosses 50 % of the range between its minimum and maximum for an individual tree in a growing season. Flower onset time was calculated as the time when flowers were first observed for an individual tree in a year. Different colors indicate NEON sites.

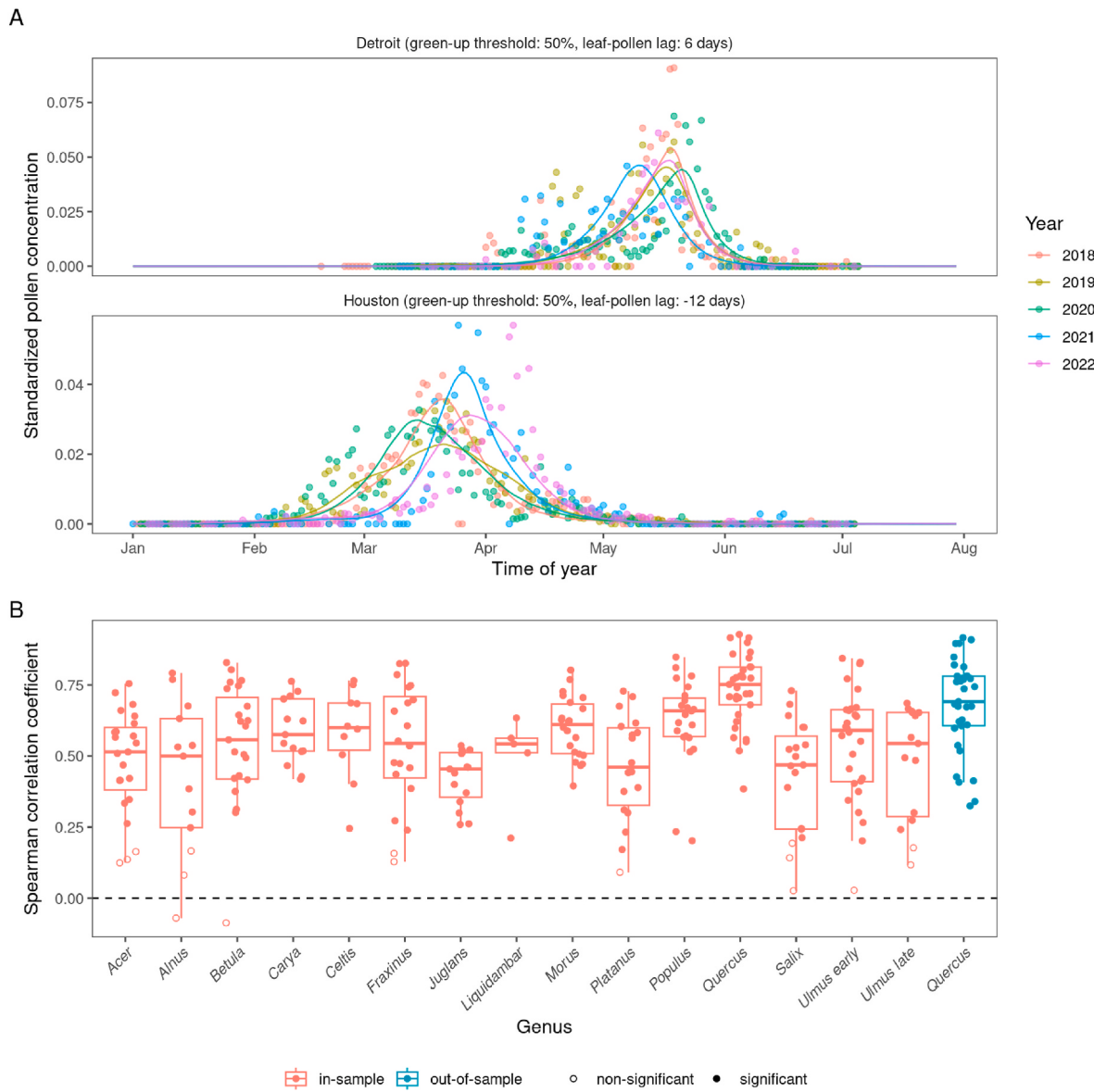


**Fig. 8.** Comparing city-level pollen phenology derived from PlanetScope and from airborne pollen concentration monitored at the National Allergy Bureau pollen monitoring stations. City-level pollen phenology is standardized pollen concentration that sum up to one for each station, year, and genus. (A) Pollen phenology inferred from PlanetScope-derived vegetative phenology tuned to the optimal green-up/down thresholds and leaf-flower lags (lines) compared to pollen phenology inferred from airborne pollen concentration (points). Pollen phenology from both data sources was standardized to probability density distribution within each city and year to allow comparison. Here we show examples of *Quercus* spp. (oak) pollen phenology in two cities in the south (Houston) and north (Detroit) of conterminous United States. (B) Accuracy of inferring pollen phenology with the PlanetScope method, both in-sample (fitting model with data from all cities) and out-of-sample (leave-one-out cross-validation), measured by Spearman correlation, indicating the level of significance ( $p \leq 0.05$ ).

different scales, we calculated the Spearman correlation coefficients.

### 2.3.3. Inferring pollen phenology on the tree level

Following the calibration of green-up/down threshold and leaf-pollen lag using NAB-derived city-level pollen phenology, we then scaled back down to infer tree-level pollen phenology using PlanetScope-derived green-up/down time  $t_{\text{green-up/down}}(\theta_g)$  (Eqn. (3)). We followed the same assumption used in the previous analysis that the time of peak pollen emission and the time of green-up/down of a tree has a time lag, optimized for each genus and city (Eqn. (8)).

$$t_{\text{pollen}} = t_{\text{green-up}}(\hat{\theta}_g) + \hat{\delta}_{gc} \quad (\text{Equation 8})$$

We were able to map the inferred peak pollen emission time of trees in a specific genus, city, and year  $t_{\text{pollen}}$ . This allowed us to summarize and visualize intra-urban variations in pollen phenology. Given that

NAB airborne concentration data used were collected at one station per city, future validation of PlanetScope-derived pollen allergy landscape with *in-situ* pollen phenology data at finer resolution is warranted.

All data analyses were performed in R v. 4.2.0 (R Core Team, 2024).

## 3. Results

### 3.1. PlanetScope-derived vegetative phenology correlates with flowering phenology

We found significant correlations between PlanetScope-derived 50 % green-up time and ground-observed flower onset time in wind-pollinated species that were well-sampled ( $\geq 50$  records) across NEON sites in conterminous United States (Fig. 7). There were significant positive correlations in six out of eight species studied, including *Acer*

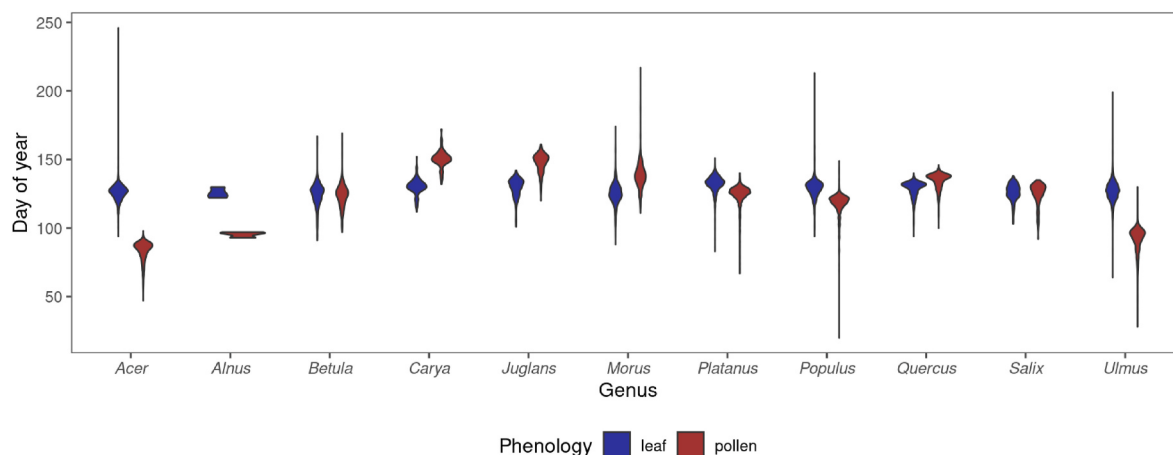


**Fig. 9.** Distributions of PlanetScope-derived tree-level spring 50 % green-up time (representing leaf phenology) and peak pollen emission time (representing pollen phenology) in Detroit in the spring of 2018. Colors indicate different genera.

*pensylvanicum* (striped maple), *Acer rubrum* (red maple), *Carya ovata* (shagbark hickory), *Liquidambar styraciflua* (sweetgum), *Quercus montana* (chestnut oak), and *Quercus rubra* (red oak). For the other two species, *Juglans nigra* (eastern American black walnut) and *Quercus stellata* (post oak), we observed no significant correlation and a significant negative correlation, respectively. Compared to strong correlation across sites, the correlation was limited within sites, where phenological variations are small. These correlations between Planet-derived green-up and ground-observed flower onset were consistent with ground-observed leaf onset and ground-observed flower onset (Fig. S8).

### 3.2. PlanetScope-derived vegetative phenology predicts city-level pollen phenology in-sample and out-of-sample

We were able to infer city-level pollen phenology from PlanetScope-derived tree-level vegetative phenology at a reasonable accuracy with optimized green-up/down thresholds for each genus and further the leaf-pollen lag for each city (Fig. 8, Figs. S9, S10, S11, S12). Among all 282 combinations of genus, city, and year, the in-sample accuracy of our PlanetScope method achieved a Spearman correlation of 0.567 (median, 95 % interval: 0.125–0.845) and a nRMSE of 14.2 % (8.81 %–33.6 %). In in-sample tests, 266 out of 282 (94.3 %) Spearman correlations were statistically significant ( $p \leq 0.05$ ). Across genera, the highest and lowest Spearman correlations were seen in *Quercus* spp. (correlation: 0.751, 0.491–0.918) and in *Juglans* spp. (correlation: 0.454, 0.260–0.531); the lowest and highest rRMSE were seen in *Liquidambar* spp. (nRMSE: 11.0 %, 8.68 %–12.7 %) and in *Alnus* spp. (nRMSE: 19.0 %, 10.7 %–23.9 %).

To test if our method can be generalized to locations without prior pollen concentration data, we performed an out-of-sample test for *Quercus* spp. that was present at seven cities, assuming a linear relationship between leaf-pollen lag and long-term climate of the city (Fig. S7). Our PlanetScope method achieved an out-of-sample Spearman correlation of 0.691 (0.337–0.910), with all 33 correlations being statistically significant, and an out-of-sample nRMSE of 14.5 % (9.82 %–36.0 %). Out-of-sample performances were comparable to in-sample performances.

We also validated in-sample PlanetScope-inferred pollen phenology with NPN-derived pollen phenology (Fig. S13). 95 out of 130 (73.1 %) Spearman correlations were statistically significant ( $p \leq 0.05$ ). The median Spearman correlation was 0.479 (−0.297–0.795), lower than the correlation with NAB-derived pollen phenology. Across genera, the highest and lowest Spearman correlations with NPN data were seen in *Acer* spp. (0.583, −0.0364–0.809) and in *Salix* spp. (0.242, 0.0371–0.664).

### 3.3. PlanetScope-derived vegetative phenology informs within-city variations in pollen phenology

Beyond the promise of extrapolating over a large spatial scale, we also explored the potential of leveraging the fine spatial resolution of PlanetScope time series to map the taxonomic and spatial details of pollen concentration within cities. Although the studied genera are similar in their time of leaf green-up, there was more heterogeneity in their time of pollen emission (Fig. 9). In addition, both the distributions of spring leaf green-up time and pollen emission time among trees of interest in a city differ from often-assumed Gaussian kernels, characterized by asymmetric peaks (Fig. 9). We mapped the inferred pollen emission among trees, showing the pollen allergy landscape with spatial variations within cities (Fig. 10).

## 4. Discussion

In this study, we developed a workflow to infer flowering and pollen phenology from PlanetScope-derived vegetative phenology, validated by *in-situ* phenological observations and measurements of airborne pollen concentrations. On the tree level, PlanetScope-derived green-up time was correlated with flower onset time. On the city level, PlanetScope-derived green-up/down time at an optimized threshold and shifted by a time lag can be used to characterize pollen phenology, with the possibility to predict out-of-sample pollen phenology in cities without pollen concentration observations. Further, we demonstrated the power of PlanetScope time series in mapping the pollen allergy landscape within cities. This study reveals the potential of high spatio-temporal resolution remote sensing data for modeling the reproductive phenology of wind-pollinated plants and mapping allergenic pollen exposures on large scales and in great spatial details.

### 4.1. Relationship between vegetative and reproductive phenology

In both tree- and city-level analyses, we showed the link between vegetative and reproductive phenology, either flower onset or pollen emission. Similar relationships have been widely supported in previous studies but on large spatial and taxonomic scales (Davies et al., 2013; Du et al., 2017; Høgda et al., 2002; Karlsen et al., 2009). However, this relationship has rarely been examined on the individual tree level (but see Primack, 1985). By comparing 50 % green-up time and flower onset time, we showed that individual trees that green up earlier also tend to flower early (Fig. 7), which may be attributed to extrinsic or intrinsic factors.

The leaf-flower correlation can be explained by shared extrinsic



**Fig. 10.** Maps of PlanetScope-derived pollen emission time in Detroit street trees in the spring of 2018, one for each genera. A brighter color indicates an earlier estimated pollen emission time from an individual tree, showing spatial heterogeneity in pollen phenology within each city and genus.

environmental conditions, as spring leaf and flower phenology respond to a common set of environmental cues (Cook et al., 2012). The optimal timing of plant life-history events in temperate ecosystems has been predicted to be constrained by the trade-off between harsh abiotic conditions and high biotic competition (CaraDonna and Bain, 2016; Iwasa and Levin, 1995; Post, 2013). This theory applies to both vegetative and reproductive phenology. The spring leaf-out of most temperate woody plant species is a result of balancing the advantages of a longer growing season with the risks from frost damage, mechanistically controlled by a suite of winter temperature, spring temperature, and photoperiod cues (Polgar and Primack, 2011). Flowers, being more sensitive than leaves to frost damage (CaraDonna and Bain, 2016), are also highly controlled by similar environmental cues (Wang et al., 2020). Shared climatic gradients can explain why remotely sensed land surface phenology was correlated with flowering and pollen season onset on a regional scale (Høgda et al., 2002; Karlsen et al., 2009). On the scale of individual trees, flowering and pollen phenology are likely to both respond to shared microclimatic conditions, such as intra-urban

temperature variation (D. S. W. Katz et al., 2019).

In addition to extrinsic factors, the leaf-flower correlation can be further explained by plants' distinct intrinsic attributes that determine their phenology (Davies et al., 2013). On a species level, these could be intrinsic species attributes such as life form, habit, dispersal mode and pollination that determine species' phenological responses to environmental cues (Davies et al., 2013), which could explain why closely related species tend to flower and leaf at similar times (i.e., phylogenetic conservatism) (Davies et al., 2013; Du et al., 2017). On an individual level, genetic differences among individuals might contribute to the leaf-flower correlation.

By revealing a leaf-flower correlation that holds on a scale smaller than previously known, we suggest the presence of fine-scale mechanisms for this correlation, either microclimatic or genetic. Such insight into the relationship between phenological events might inform the integration of leaf phenology in the mechanistic model for flower and pollen phenology.

#### 4.2. Detecting tree-level phenology with PlanetScope

Validated by *in-situ* phenological observations, we closely examined the often-assumed potential of PlanetScope to detect tree-level phenology (Cheng et al., 2020; Wu et al., 2021; Zhao et al., 2022). Across NEON sites, PlanetScope-derived phenometrics captured tree-level variations in the onset of maple and oak flowers. This result is consistent with the finding that PlanetScope-derived phenometrics explained tree-level variations in the leaf onset time of deciduous trees across NEON sites (Zhao et al., 2022) and in leaf senescence time at a PhenoCam site in a temperate forest (Wu et al., 2021).

Nevertheless, we noted that tree-level correlations were contributed mainly by cross-site rather than within-site correlations (Fig. 7). The weak within-site correlations were also observed in Zhao et al. (2022) and were explained with both the uncertainty of extracting phenometrics from PlanetScope time series and inconsistencies in field phenological observations. An additional reason is that the correlations between leaf onset time and flower onset time, a premise of our method, might be weaker within the site compared to across sites (Fig. S7).

The ability to detect tree-level phenology using PlanetScope time series is highly relevant from both a scientific and a practical standpoint. On one hand, there are large variations between the phenology of trees within a population, often with a conserved order of phenological events among trees repeating from year to year, referred to as “phenological rank” (Delpierre et al., 2017). Such tree-level phenological variations could arise from multiple factors, including phenological variations in phenotype, microclimate, and local resource availability (Vitasse et al., 2021). PlanetScope-derived phenology will allow a better understanding of ecological factors that underlie phenology. In practice, tree-level variations in pollen phenology contribute to spatial heterogeneity of pollen concentration within a city (D. S. W. Katz et al., 2019).

While current pollen concentration data and pollen models are largely confined to regional or city scales, PlanetScope-derived pollen phenology has the potential to empower process-guided pollen models with a higher spatial resolution. Here, we demonstrate how our PlanetScope-derived green-up time tuned to the optimal thresholds and lags, integrated with street-tree inventory, allowed us to map the spatial heterogeneity of PlanetScope-derived pollen emission time in a given city and time (Fig. 10). Such maps showing intra-urban phenological variations can inform decision-making such as time and location of outdoor activities. Future validation with spatiotemporal pollen phenology data on sub-city scales is warranted (Zapata-Marin et al., 2022).

The method we employed to extract tree-level phenology here using coordinates of censused trees combined with PlanetScope is highly scalable, but limitations remain given uncertainties in effective footprint size and geolocation accuracy of PlanetScope pixels. Small trees (e.g., with a canopy diameter <3 m) might not be suitable to be extracted for the phenological signal from PlanetScope. The size of trees could be controlled if there exists information on tree diameter, height, or age in tree inventories; alternatively, this could be achieved by segmentation of tree canopy. Manual segmentation of tree crowns from drone imagery has been used to delineate polygons to extract phenological signals from PlanetScope (Wu et al., 2021; Zhao et al., 2022). Such tree crown segmentation could be automated in the presence of co-registered airborne RGB, LiDAR hyperspectral imagery, and high-quality training data (Weinstein et al., 2021).

#### 4.3. Using PlanetScope time series to inform pollen phenology

In the city-level analysis using pollen concentration data, we proposed a novel workflow to predict pollen phenology from PlanetScope time series. We compared the performance of our method to previous machine learning models that do not explicitly account for phenology and a study that directly accounts for flowering phenology. On the one hand, our in-sample nRMSE of 14.2 % and out-of-sample nRMSE of 14.5 % (for *Quercus* spp. only) were highly competitive with machine

learning models with nRMSE generally above 20 % (Seo et al., 2019; Makra et al., 2023), even though our model had very few parameters (Supplementary Note) and we did not include any environmental predictors to account for climate or weather changes. On the other hand, our performance was comparable to or better than that of process-based models. For example, the System for Integrated modeling of Atmospheric composition (SILAM), a widely-used process-based modeling system in Europe (Sofiev et al., 2024), gave an nRMSE of approximately 20 % in pollen prediction (Sofiev et al., 2015). The Environment – High Resolution Limited Area Model (Enviro-HIRLAM) predicted birch pollen over Europe with RMSE of 1223.95–1639.47 pollen m<sup>-3</sup>, translating to nRMSE of 12.2–16.4 %, assuming a maximum pollen concentration of 10<sup>4</sup> pollen m<sup>-3</sup> (Kurganskiy et al., 2020). Further, we outperformed a previous study that predicted the same NAB pollen concentration dataset with *in-situ* flower observations collected by community scientist volunteers (Crimmins et al., 2023). We achieved higher and more statistically significant Spearman correlations in this study: 58 % and 94.3 % of Spearman correlations were statistically significant in Crimmins et al. (2023) and this study, respectively; the median Spearman correlation for *Quercus* spp. was 0.49 and 0.751 in Crimmins et al. (2023) and this study, respectively. When benchmarked against an alternative data source from citizen science (Fig. S13), the accuracy of our method is slightly lower (73.1 % Spearman correlations being statistically significant), which might be due to the spatiotemporal biases of data contribution. The competitive performance of our model demonstrated the power of phenology data in pollen models and the great potential of PlanetScope-derived phenology data.

The accuracy of our method arises from the ability of PlanetScope-derived pollen phenology to explain intra-annual and inter-annual variations in pollen concentration. By empirically inferring the continuous change in pollen phenology in a year from the distribution of green-up/down days among trees (Fig. 8), we moved beyond traditional pollen phenology modeling that relies on annual phenometrics (Clark et al., 2014). Even without explicitly accounting for inter-annual variations in temperature, the PlanetScope method was able to explain some inter-annual variations in pollen phenology with the different times and distributions of green-up/down dates (Fig. 8, Fig. S10). This finding has previously been shown on a coarser resolution, with a remotely-sensed green-up date explaining inter-annual variations in ground-observed flowering dates (Delbart et al., 2015).

Our model was a simplified one, overlooking details such as differential responses of vegetative and reproductive phenology to the environment (Geng et al., 2022) and non-phenological factors that influence pollen concentration, such as pollen dispersion (Latorre, 1999; Robichaud and Comtois, 2021; Zhu et al., 2024). Nevertheless, this model paves the way for building process-guided pollen models with tree-level vegetative and reproductive phenology as key processes (Scheifinger et al., 2013; D. S. W. Katz et al., 2023).

The out-of-sample accuracy of PlanetScope-derived pollen phenology of oak trees (Fig. 8, Fig. S11) suggested the possibility of predicting pollen concentration even at locations with limited prior observations. We suggest four enhancements before operationalizing the proposed workflow to inform decision-making in public health. First, in addition to the tree-level validation of the flowering phenology we presented, more fine-scale ground truths for pollen phenology are needed (Katz and Batterman, 2020). Examples are newly initiated community science data collection of pollen phenology (D. S. W. Katz et al., 2023) and within-city pollen concentration data (Weinberger et al., 2018). Second, our study was partly limited by the number of cities with publicly available street inventories. To ensure a sufficient number of cities for extrapolation, we were not able to perform out-of-sample tests with genera other than *Quercus* spp. Further model tuning and validation will benefit from obtaining street tree inventories from more cities. Apart from direct requests from cities, operationalized identification of trees with remote sensing data (Morueta-Holme et al., 2024), such as the Auto Arborist dataset (Beery et al., 2022), may be

particularly efficient. Third, by focusing on phenology, our method addressed the relative change of pollen concentration but not the absolute magnitude of pollen peaks, which can be achieved by accounting for the total pollen production per tree and abundance and distribution of the taxa of interest (D. S. W. Katz and Carey, 2014; D. S. W. Katz et al., 2020; Zhang and Steiner, 2022). Last, although this study retrospectively demonstrates the inference of pollen phenology, this method can be combined with accurate forecasting of vegetative phenology (Song et al., 2023; Taylor and White, 2020) to achieve near-term predictions for the early warning of pollen season. With around 60 pollen monitoring stations around the US but far more widespread public health concerns on pollen allergy, this study provides the possibility of more spatially equitable access to pollen level forecasting.

## 5. Conclusions

We showed that high spatiotemporal resolution remote sensing data from PlanetScope is highly promising in inferring flowering and pollen phenology from vegetative phenology. On the tree level, PlanetScope-derived green-up time had a significant positive correlation with the field-observed flower onset time of six out of eight wind-pollinated species in a large observatory network (Section 3.1). We upscaled tree-level PlanetScope-derived vegetative phenology to the city level and accurately inferred pollen phenology, calibrated by a conterminous-scale high-quality dataset for airborne pollen concentration (Section 3.2). This empirical method of inference achieved a median Spearman correlation of 0.567 and a nRMSE of 14.2 % across 14 wind-pollinated genera and seven cities of interest. For *Quercus* spp. (oak) that was present in all seven cities; our model achieved high out-of-sample accuracy (Spearman correlation: 0.691, nRMSE: 14.5 %) comparable with in-sample accuracy (Spearman correlation: 0.751, nRMSE: 13.5 %). Our proposed method is promising to describe and predict the pollen phenology of deciduous wind-pollinated tree taxa at locations without prior pollen concentration data. We further demonstrate how PlanetScope-derived vegetative phenology can be used to map variations in pollen phenology within cities (a pollen allergy landscape) (Section 3.3), calling for future validation with fine-grained *in-situ* data. Using PlanetScope time series, our findings pave the way for the development of generalizable and refined process-based pollen models to inform decision-making in public health.

## CRediT authorship contribution statement

**Yiluan Song:** Writing – review & editing, Writing – original draft, Methodology, Formal analysis, Data curation, Conceptualization. **Daniel S.W. Katz:** Writing – review & editing, Data curation, Conceptualization. **Zhe Zhu:** Writing – review & editing, Methodology, Conceptualization. **Claudie Beaulieu:** Writing – review & editing, Methodology, Conceptualization. **Kai Zhu:** Writing – review & editing, Supervision, Resources, Conceptualization.

## Data availability

We retrieved ground-observed plant phenology data (DP1.10055.001) from the National Ecological Observatory Network (NEON) integrated into the USA National Phenology Network (USA-NPN) using R package *rmpn* on Feb 1, 2024. We obtained pollen concentration data from pollen monitoring stations associated with the National Allergy Bureau. Pollen concentration data were received on Apr 25, 2023 and will not be released due to confidentiality reasons. We downloaded PlanetScope imagery for areas of interest through the Planet API, adapting an R package *planetR*, during Feb 1, 2024–Mar 14, 2024. Processed data and novel R code are permanently archived on Zenodo <https://doi.org/10.5281/zenodo.15080735>. A walk-through of our analysis is available on our project website <https://bookdown.org/yiluansong/RS4flower/>. More figures on results can be visualized

interactively on our R Shiny app ([https://yiluansong.shinyapps.io/RS4flower\\_result/](https://yiluansong.shinyapps.io/RS4flower_result/)).

## Declaration of competing interest

The authors declare that they have no known competing financial interests or personal relationships that could have appeared to influence the work reported in this paper.

## Acknowledgments

The authors would like to thank Drs. Yang Chen and Inés Ibáñez, and members of the Zhu Lab at the University of Michigan, for comments on the manuscript. Yiluan Song was supported by the UCSC Hammett Fellowship, the Microsoft AI for Earth Grant, and the Eric and Wendy Schmidt AI in Science Postdoctoral Fellowship, a Schmidt Sciences program. Kai Zhu and Yiluan Song were supported by the National Science Foundation [grant numbers 2306198 (CAREER)] and Michigan Institute for Data and AI in Society. This work was supported by the USDA McIntire-Stennis Capacity Grant Program under Award Number 25-PAF01509.

## Appendix A. Supplementary data

Supplementary data to this article can be found online at <https://doi.org/10.1016/j.srs.2025.100205>.

## Data availability

Processed data and novel R code are permanently archived on Zenodo <https://doi.org/10.5281/zenodo.15080735>. A walk-through of our analysis is available on our project website <https://bookdown.org/yiluansong/RS4flower/>.

## References

- AAAI, 2022. NAB data release guidelines. <https://www.aaai.org/Aaaai/media/MediaLibrary/PDF%20Documents/NAB/NAB-Data-Release-Guidelines-Final-7-24-13.pdf>.
- Abatzoglou, J.T., Dobrowski, S.Z., Parks, S.A., Hegewisch, K.C., 2018. TerraClimate, a high-resolution global dataset of monthly climate and climatic water balance from 1958–2015. Sci. Data 5 (1), 1. <https://doi.org/10.1038/sdata.2017.191>.
- Anderegg, W.R.L., Abatzoglou, J.T., Anderegg, L.D.L., Bielory, L., Kinney, P.L., Ziska, L., 2021. Anthropogenic climate change is worsening North American pollen seasons. Proc. Natl. Acad. Sci. USA 118 (7). <https://doi.org/10.1073/pnas.2013284118>.
- Bastl, K., Kminta, M., Berger, M., Berger, U., 2018. The connection of pollen concentrations and crowd-sourced symptom data: New insights from daily and seasonal symptom load index data from 2013 to 2017 in Vienna. The World Allergy Organization Journal 11 (1), 24. <https://doi.org/10.1186/s40413-018-0203-6>.
- Bastl, M., Bastl, K., Dirr, L., Berger, M., Berger, U., 2023. Methods and standards of pollen monitoring—significance of pollen measurements at different altitudes. Allergo Journal International 32 (6), 162–166. <https://doi.org/10.1007/s40629-023-00268-3>.
- Beaulieu, C., Killick, R., 2018. Distinguishing trends and shifts from memory in climate data. J. Clim. 31 (23), 9519–9543. <https://doi.org/10.1175/JCLI-D-17-0863.1>.
- Beery, S., Wu, G., Edwards, T., Pavetic, F., Majewski, B., Mukherjee, S., Chan, S., Morgan, J., Rathod, V., Huang, J., 2022. The Auto Arborist dataset: a large-scale benchmark for multiview urban forest monitoring under domain shift, 21294–21307. [https://openaccess.thecvf.com/content/CVPR2022/html/Beery\\_The\\_Auto\\_Arborist\\_Dataset\\_A\\_Large-Scale\\_Benchmark\\_for\\_Multiview\\_Urban\\_CVPR\\_2022\\_paper.html](https://openaccess.thecvf.com/content/CVPR2022/html/Beery_The_Auto_Arborist_Dataset_A_Large-Scale_Benchmark_for_Multiview_Urban_CVPR_2022_paper.html).
- Bevington, A., Tobias, M., Nelsen, T., Stockwell, E., 2024. *planetR* [R]. <https://github.com/bevingtona/planetR> (Original work published 2019).
- Bonini, M., Monti, G.S., Pelagatti, M.M., Ceriotti, V., Re, E.E., Bramè, B., Bottero, P., Tosi, A., Vaghi, A., Martelli, A., Traina, G.M., Rivolta, L., Rivolta, F., Ortolani, C.M., 2022. Ragweed pollen concentration predicts seasonal rhino-conjunctivitis and asthma severity in patients allergic to ragweed. Sci. Rep. 12 (1), 1. <https://doi.org/10.1038/s41598-022-20069-y>.
- Buonaiuto, D.M., Morales-Castilla, I., Wolkovich, E.M., 2021. Reconciling competing hypotheses regarding flower–leaf sequences in temperate forests for fundamental and global change biology. New Phytol. 229 (3), 1206–1214. <https://doi.org/10.1111/nph.16848>.
- Buonaiuto, D.M., Wolkovich, E.M., 2021. Differences between flower and leaf phenological responses to environmental variation drive shifts in spring

- phenological sequences of temperate woody plants. *J. Ecol.* 109 (8), 2922–2933. <https://doi.org/10.1111/1365-2745.13708>.
- Campbell, T., Fearn, P., 2018. Simple remote sensing detection of *Corymbia calophylla* flowers using common 3-band imaging sensors. *Remote Sens. Appl.: Society and Environment* 11, 51–63. <https://doi.org/10.1016/j.rsa.2018.04.009>.
- CaraDonna, P.J., Bain, J.A., 2016. Frost sensitivity of leaves and flowers of subalpine plants is related to tissue type and phenology. *J. Ecol.* 104 (1), 55–64. <https://doi.org/10.1111/1365-2745.12482>.
- Chamberlain, S.A., Szöcs, E., 2013. taxize: taxonomic search and retrieval in R. *F1000Research* 2, 191. <https://doi.org/10.12688/f1000research.2-191.v2>.
- Chen, B., Jin, Y., Brown, P., 2019. An enhanced bloom index for quantifying floral phenology using multi-scale remote sensing observations. *ISPRS J. Photogrammetry Remote Sens.* 156, 108–120. <https://doi.org/10.1016/j.isprsjprs.2019.08.006>.
- Chen, X., Wang, D., Chen, J., Wang, C., Shen, M., 2018. The mixed pixel effect in land surface phenology: a simulation study. *Rem. Sens. Environ.* 211, 338–344. <https://doi.org/10.1016/j.rse.2018.04.030>.
- Cheng, Y., Vrieling, A., Fava, F., Meroni, M., Marshall, M., Gachoki, S., 2020. Phenology of short vegetation cycles in a Kenyan rangeland from PlanetScope and Sentinel-2. *Rem. Sens. Environ.* 248, 112004. <https://doi.org/10.1016/j.rse.2020.112004>.
- Chuine, I., Belmonte, J., 2004. Improving prophylaxis for pollen allergies: predicting the time course of the pollen load of the atmosphere of major allergenic plants in France and Spain. *Grana* 43 (2), 65–80. <https://doi.org/10.1080/00173130410019163>.
- Clark, J.S., Salk, C., Melillo, J., Mohan, J., 2014. Tree phenology responses to winter chilling, spring warming, at north and south range limits. *Funct. Ecol.* 28 (6), 1344–1355. <https://doi.org/10.1111/1365-2435.12309>.
- Cook, B.I., Wolkovich, E.M., Davies, T.J., Ault, T.R., Betancourt, J.L., Allen, J.M., Bolmgren, K., Cleland, E.E., Crimmins, T.M., Kraft, N.J.B., Lancaster, L.T., Mazer, S.J., McCabe, G.J., McGill, B.J., Parmesan, C., Pau, S., Regetz, J., Salamin, N., Schwartz, M.D., Travers, S.E., 2012. Sensitivity of spring phenology to warming across temporal and spatial climate gradients in two independent databases. *Ecosystems* 15 (8), 1283–1294. <https://doi.org/10.1007/s10021-012-9584-5>.
- Crimmins, T.M., Crimmins, M.A., Gerst, K.L., Rosemarin, A.H., Weltzin, J.F., 2017. USA National Phenology Network's volunteer-contributed observations yield predictive models of phenological transitions. *PLoS One* 12 (8), e0182919. <https://doi.org/10.1371/journal.pone.0182919>.
- Crimmins, T.M., Vogt, E., Brown, C.L., Dalan, D., Manangan, A., Robinson, G., Song, Y., Zhu, K., Katz, D.S.W., 2023. Volunteer-contributed observations of flowering often correlate with airborne pollen concentrations. *Int. J. Biometeorol.* 67 (8), 1363–1372. <https://doi.org/10.1007/s00484-023-02506-3>.
- Crisp, H.C., Gomez, R.A., White, K.M., Quinn, J.M., 2013. A side-by-side comparison of Rotorod and Burkard pollen and spore collections. *Ann. Allergy Asthma Immunol.* 111 (2), 118–125. <https://doi.org/10.1016/j.anai.2013.05.021>.
- Dahl, Å., Galán, C., Hajkova, L., Pauling, A., Sikoparija, B., Smith, M., Vokou, D., 2013. The onset, course and intensity of the pollen season. In: Sofiev, M., Bergmann, K.-C. (Eds.), *Allergenic Pollen: A Review of the Production, Release, Distribution and Health Impacts*. Springer, Netherlands, pp. 29–70. [https://doi.org/10.1007/978-94-007-4881-1\\_3](https://doi.org/10.1007/978-94-007-4881-1_3).
- D'Amato, G., Chong-Neto, H.J., Monge Ortega, O.P., Vitale, C., Ansotegui, I., Rosario, N., Haahtelä, T., Galan, C., Pawankar, R., Muñoz-Aguttes, M., Cecchi, L., Bergmann, C., Ridolo, E., Ramon, G., Gonzalez Diaz, S., D'Amato, M., Annesi-Maesano, I., 2020. The effects of climate change on respiratory allergy and asthma induced by pollen and mold allergens. *Allergy* 75 (9), 2219–2228. <https://doi.org/10.1111/all.14476>.
- Davies, T.J., Wolkovich, E.M., Kraft, N.J.B., Salamin, N., Allen, J.M., Ault, T.R., Betancourt, J.L., Bolmgren, K., Cleland, E.E., Cook, B.I., Crimmins, T.M., Mazer, S.J., McCabe, G.J., Pau, S., Regetz, J., Schwartz, M.D., Travers, S.E., 2013. Phylogenetic conservatism in plant phenology. *J. Ecol.* 101 (6), 1520–1530. <https://doi.org/10.1111/1365-2745.12154>.
- Delbart, N., Beaubien, E., Kergoat, L., Le Toan, T., 2015. Comparing land surface phenology with leafing and flowering observations from the PlantWatch citizen network. *Rem. Sens. Environ.* 160, 273–280. <https://doi.org/10.1016/j.rse.2015.01.012>.
- Delpierre, N., Guillemot, J., Dufrêne, E., Cecchini, S., Nicolas, M., 2017. Tree phenological ranks repeat from year to year and correlate with growth in temperate deciduous forests. *Agric. For. Meteorol.* 234–235, 1–10. <https://doi.org/10.1016/j.agrformet.2016.12.008>.
- Denny, E.G., Gerst, K.L., Miller-Rushing, A.J., Tierney, G.L., Crimmins, T.M., Enquist, C.A.F., Guertin, P., Rosemarin, A.H., Schwartz, M.D., Thomas, K.A., Weltzin, J.F., 2014. Standardized phenology monitoring methods to track plant and animal activity for science and resource management applications. *Int. J. Biometeorol.* 58 (4), 591–601. <https://doi.org/10.1007/s00484-014-0789-5>.
- Dixon, D.J., Callow, J.N., Duncan, J.M.A., Setterfield, S.A., Pauli, N., 2021. Satellite prediction of forest flowering phenology. *Rem. Sens. Environ.* 255, 112197. <https://doi.org/10.1016/j.rse.2020.112197>.
- Dixon, D.J., Zhu, Y., Brown, C.F., Jin, Y., 2023. Satellite detection of canopy-scale tree mortality and survival from California wildfires with spatio-temporal deep learning. *Rem. Sens. Environ.* 298, 113842. <https://doi.org/10.1016/j.rse.2023.113842>.
- Donnelly, A., Yu, R., Jones, K., Belitz, M., Li, B., Duffy, K., Zhang, X., Wang, J., Seyednasrollah, B., Gerst, K.L., Li, D., Kadoura, Y., Zhu, K., Morisette, J., Ramey, C., Smith, K., 2022. Exploring discrepancies between in situ phenology and remotely derived phenometrics at NEON sites. *Ecosphere* 13 (1), e3912. <https://doi.org/10.1002/ecs2.3912>.
- Du, Y., Chen, J., Willis, C.G., Zhou, Z., Liu, T., Dai, W., Zhao, Y., Ma, K., 2017. Phylogenetic conservatism and trait correlates of spring phenological responses to climate change in northeast China. *Ecol. Evol.* 7 (17), 6747–6757. <https://doi.org/10.1002/ee.3.3207>.
- Eilers, P.H.C., 2003. A perfect smoother. *Anal. Chem.* 75 (14), 3631–3636. <https://doi.org/10.1021/ac034173t>.
- Eilers, P.H.C., 2004. Parametric time warping. *Anal. Chem.* 76 (2), 404–411. <https://doi.org/10.1021/ac034800e>.
- Elmendorf, S.C., Jones, K.D., Cook, B.I., Diez, J.M., Enquist, C.A.F., Hufft, R.A., Jones, M.O., Mazer, S.J., Miller-Rushing, A.J., Moore, D.J.P., Schwartz, M.D., Weltzin, J.F., 2016. The plant phenology monitoring design for the National Ecological Observatory Network. *Ecosphere* 7 (4), e01303. <https://doi.org/10.1002/ecs2.1303>.
- Frenguelli, G., Bricchi, E., Romano, B., Mincigrucci, G., Spieksma, F. Th M., 1989. A predictive study on the beginning of the pollen season for Gramineae andolea europaea L. *Aerobiologia* 5 (1), 64–70. <https://doi.org/10.1007/BF02446489>.
- Frenz, D.A., 1999. Comparing pollen and spore counts collected with the Rotorod Sampler and Burkard spore trap. *Ann. Allergy Asthma Immunol.* 83 (5), 341–349. [https://doi.org/10.1016/S1081-1206\(10\)62828-1](https://doi.org/10.1016/S1081-1206(10)62828-1).
- Galán, C., Smith, M., Thibaudon, M., Frenguelli, G., Oteros, J., Gehrig, R., Berger, U., Clot, B., Brando, R., EAS QC Working Group, 2014. Pollen monitoring: minimum requirements and reproducibility of analysis. *Aerobiologia* 30 (4), 385–395. <https://doi.org/10.1007/s10453-014-9335-5>.
- García-Mozo, H., Galán, C., Belmonte, J., Bermejo, D., Candau, P., Díaz de la Guardia, C., Elvira, B., Gutierrez, M., Jato, V., Silva, I., Trigo, M.M., Valencia, R., Chuine, I., 2009. Predicting the start and peak dates of the Poaceae pollen season in Spain using process-based models. *Agric. For. Meteorol.* 149 (2), 256–262. <https://doi.org/10.1016/j.agrformet.2008.08.013>.
- Geng, X., Fu, Y.H., Piao, S., Hao, F., De Boec, H.J., Zhang, X., Chen, S., Guo, Y., Prevéy, J.S., Vitassee, Y., Peníuelas, J., Janssens, I.A., Stenseth, N. Chr., 2022. Higher temperature sensitivity of flowering than leaf-out alters the time between phenophases across temperate tree species. *Global Ecol. Biogeogr.* 31 (5), 901–911. <https://doi.org/10.1111/geb.13463>.
- Guo, L., Liu, X., Alatalo, J.M., Wang, C., Xu, J., Yu, H., Chen, J., Yu, Q., Peng, C., Dai, J., Luedeling, E., 2023. Climatic drivers and ecological implications of variation in the time interval between leaf-out and flowering. *Curr. Biol.* 33 (16), 3338–3349.e3. <https://doi.org/10.1016/j.cub.2023.06.064>.
- Høgda, K.A., Karlsen, S.R., Solheim, I., Tommervik, H., Ramfjord, H., 2002. The start dates of birch pollen seasons in Fennoscandia studied by NOAA AVHRR NDVI data. *IEEE International Geoscience and Remote Sensing Symposium* 6, 3299–3301. <https://doi.org/10.1109/IGARSS.2002.1027162>.
- Huete, A., Tran, N.N., Nguyen, H., Xie, Q., Katalaris, C., 2019. Forecasting pollen aerobiology with MODIS EVI, land cover, and phenology using machine learning tools. *IGARSS 2019 - 2019 IEEE International Geoscience and Remote Sensing Symposium* 5429–5432. <https://doi.org/10.1109/IGARSS.2019.8898796>.
- Idrose, N.S., Lodge, C.J., Erbas, B., Douglass, J.A., Bui, D.S., Dharmage, S.C., 2022. A review of the respiratory health burden attributable to short-term exposure to pollen. *Int. J. Environ. Res. Publ. Health* 19 (12), 12. <https://doi.org/10.3390/ijerph19127541>.
- Immler, F., Tziastas, P., 2024. Horizon projects using environmental observations and artificial intelligence for the benefit of science and society. In: Immler, F., Tziastas, P. (Eds.), European Commission: Directorate-General for Research and Innovation. Publications Office of the European Union. <https://data.europa.eu/doi/10.2777/167982>.
- Iwasa, Y., Levin, S.A., 1995. The timing of life history events. *J. Theor. Biol.* 172 (1), 33–42. <https://doi.org/10.1006/jtbi.1995.0003>.
- Jeon, W., Choi, Y., Roy, A., Pan, S., Price, D., Hwang, M.-K., Kim, K.R., Oh, I., 2018. Investigation of primary factors affecting the variation of modeled oak pollen concentrations: a case study for southeast Texas in 2010. *Asia-Pacific Journal of Atmospheric Sciences* 54 (1), 33–41. <https://doi.org/10.1007/s13143-017-0057-9>.
- Karlsen, S.R., Ramfjord, H., Høgda, K.A., Johansen, B., Danks, F.S., Brobakk, T.E., 2008. A satellite-based map of onset of birch (*Betula*) flowering in Norway. *Aerobiologia* 25 (1), 15. <https://doi.org/10.1007/s10453-008-9105-3>.
- Karlsen, S.R., Ramfjord, H., Høgda, K.A., Johansen, B., Danks, F.S., Brobakk, T.E., 2009. A satellite-based map of onset of birch (*Betula*) flowering in Norway. *Aerobiologia* 25 (1), 15–25. <https://doi.org/10.1007/s10453-008-9105-3>.
- Katz, D., Edwards, K., Huang, S., Robinson, G., 2024. Quantifying pollen forecast accuracy: an assessment of private sector predictions in New York. *J. Allergy Clin. Immunol.* 153 (2), AB109. <https://doi.org/10.1016/j.jaci.2023.11.355>.
- Katz, D.S.W., Baptist, A.P., Batterman, S.A., 2023a. Modeling airborne pollen concentrations at an urban scale with pollen release from individual trees. *Aerobiologia* 39 (2), 181–193. <https://doi.org/10.1007/s10453-023-09784-9>.
- Katz, D.S.W., Batterman, S.A., 2020. Urban-scale variation in pollen concentrations: a single station is insufficient to characterize daily exposure. *Aerobiologia* 36 (3), 417–431. <https://doi.org/10.1007/s10453-020-09641-z>.
- Katz, D.S.W., Carey, T.S., 2014. Heterogeneity in ragweed pollen exposure is determined by plant composition at small spatial scales. *Sci. Total Environ.* 485–486, 435–440. <https://doi.org/10.1016/j.scitotenv.2014.03.099>.
- Katz, D.S.W., Dzul, A., Kendel, A., Batterman, S.A., 2019. Effect of intra-urban temperature variation on tree flowering phenology, airborne pollen, and measurement error in epidemiological studies of allergenic pollen. *Sci. Total Environ.* 653, 1213–1222. <https://doi.org/10.1016/j.scitotenv.2018.11.020>.
- Katz, D.S.W., Morris, J.R., Batterman, S.A., 2020. Pollen production for 13 urban North American tree species: allometric equations for tree trunk diameter and crown area. *Aerobiologia* 36 (3), 401–415. <https://doi.org/10.1007/s10453-020-09638-8>.
- Katz, D.S.W., Vogt, E., Manangan, A., Brown, C.L., Dalan, D., Zhu, K., Song, Y., Crimmins, T.M., 2023b. Observations from the USA National Phenology Network can be leveraged to model airborne pollen. *Aerobiologia* 39 (1), 169–174. <https://doi.org/10.1007/s10453-022-09774-3>.

- Kim, I., Kwak, M.J., Lee, J.K., Lim, Y., Park, S., Kim, H., Lee, K.-A., Woo, S.Y., 2020. Flowering phenology and characteristics of pollen aeroparticles of *Quercus* species in Korea. *Forests* 11 (2), 2. <https://doi.org/10.3390/f11020232>.
- Kington, J., Collison, A., 2022. Scene level normalization and harmonization of Planet Dove imagery. Planet. [https://assets.planet.com/docs/scene\\_level\\_normalization\\_of\\_planet\\_dove\\_imagery.pdf](https://assets.planet.com/docs/scene_level_normalization_of_planet_dove_imagery.pdf).
- Kong, D., Zhang, Y., Gu, X., Wang, D., 2019. A robust method for reconstructing global MODIS EVI time series on the Google Earth Engine. *ISPRS J. Photogrammetry Remote Sens.* 155, 13–24. <https://doi.org/10.1016/j.isprsjprs.2019.06.014>.
- Kurganskiy, A., Skjøth, C.A., Baklanov, A., Sofiev, M., Saarto, A., Severova, E., Smyslyeva, S., Kaas, E., 2020. Incorporation of pollen data in source maps is vital for pollen dispersion models. *Atmos. Chem. Phys.* 20 (4), 2099–2121. <https://doi.org/10.5194/acp-20-2099-2020>.
- Latorre, F., 1999. Differences between airborne pollen and flowering phenology of urban trees with reference to production, dispersal and interannual climate variability. *Aerobiologia* 15 (2), 131–141. <https://doi.org/10.1023/A:100752316024>.
- Levetin, E., McLoud, J.D., Pitny, P., Rorie, A.C., 2023. Air sampling and analysis of aeroallergens: current and future approaches. *Curr. Allergy Asthma Rep.* 23 (5), 223–236. <https://doi.org/10.1007/s11882-023-01073-2>.
- Liú, H.Q., Huete, A., 1995. A feedback based modification of the NDVI to minimize canopy background and atmospheric noise. *IEEE Trans. Geosci. Rem. Sens.* 33 (2), 457–465. <https://doi.org/10.1109/TGRS.1995.8746027>. IEEE Transactions on Geoscience and Remote Sensing.
- Liú, Y., Zhang, X., Shen, Y., Ye, Y., Gao, S., Tran, K.H., 2024. Evaluation of PlanetScope-detected plant-specific phenology using infrared-enabled PhenoCam observations in semi-arid ecosystems. *ISPRS J. Photogrammetry Remote Sens.* 210, 242–259. <https://doi.org/10.1016/j.isprsjprs.2024.03.017>.
- Lo, F.A., 2020. Understanding And Forecasting Allergenic Pollen in the United States. Ph.D., University of Washington. <https://search.proquest.com/docview/2437811739/abstract/4254BA86F3B54ACBPQ/1>.
- Lo, F., Bitz, C.M., Battisti, D.S., Hess, J.J., 2019. Pollen calendars and maps of allergenic pollen in North America. *Aerobiologia* 35 (4), 613–633. <https://doi.org/10.1007/s10453-019-09601-2>.
- Lo, F., Bitz, C.M., Hess, J.J., 2021. Development of a Random Forest model for forecasting allergenic pollen in North America. *Sci. Total Environ.* 773, 145590. <https://doi.org/10.1016/j.scitotenv.2021.145590>.
- Ma, Q., Huang, J.-G., Hänninen, H., Li, X., Berninger, F., 2021. Climate warming prolongs the time interval between leaf-out and flowering in temperate trees: effects of chilling, forcing and photoperiod. *J. Ecol.* 109 (3), 1319–1330. <https://doi.org/10.1111/1365-2745.13558>.
- Makra, L., Matyasovszky, I., Tüsnyády, G., Ziská, L.H., Hess, J.J., Nyúl, L.G., Chapman, D. S., Covillejo, L., Gobbi, A., Jurman, G., Furlanello, C., Brunato, M., Damialis, A., Charalampopoulos, A., Müller-Schärer, H., Schneider, N., Szabó, B., Sümeghy, Z., Páldy, A., et al., 2023. A temporally and spatially explicit, data-driven estimation of airborne ragweed pollen concentrations across Europe. *Sci. Total Environ.* 905, 167095. <https://doi.org/10.1016/j.scitotenv.2023.167095>.
- Maya-Manzano, J.M., Smith, M., Markey, E., Hourihane Clancy, J., Sodeau, J., O'Connor, D.J., 2021. Recent developments in monitoring and modelling airborne pollen, a review. *Grana* 60 (1), 1–19. <https://doi.org/10.1080/00173134.2020.1769176>.
- Mimić, G., Podraščanin, Z., Lugojan, P., Šikoparija, B., 2021. The influence of source maps on SILAM performance in modeling ragweed pollen concentrations in the area of a major European source. *Int. J. Biometeorol.* 65 (6), 917–928. <https://doi.org/10.1007/s00484-021-02075-3>.
- Mo, F., Zhang, J., Wang, J., Cheng, Z.-G., Sun, G.-J., Ren, H.-X., Zhao, X.-Z., Cheruiyot, W.K., Kavagi, L., Wang, J.-Y., Xiong, Y.-C., 2017. Phenological evidence from China to address rapid shifts in global flowering times with recent climate change. *Agric. For. Meteorol.* 246, 22–30. <https://doi.org/10.1016/j.agrformet.2017.06.004>.
- Moon, M., Richardson, A.D., Friedl, M.A., 2021. Multiscale assessment of land surface phenology from harmonized Landsat 8 and Sentinel-2, PlanetScope, and PhenoCam imagery. *Rem. Sens. Environ.* 266, 112716. <https://doi.org/10.1016/j.rse.2021.112716>.
- Moon, M., Richardson, A.D., Milliman, T., Friedl, M.A., 2022. A high spatial resolution land surface phenology dataset for AmeriFlux and NEON sites. *Sci. Data* 9 (1), 1. <https://doi.org/10.1038/s41597-022-01570-5>.
- Morueta-Holme, N., Iversen, L.L., Corcoran, D., Rahbek, C., Normand, S., 2024. Unlocking ground-based imagery for habitat mapping. *Trends Ecol. Evol.* 39 (4), 349–358. <https://doi.org/10.1016/j.tree.2023.11.005>.
- Muggeo, V.M.R., 2008. Segmented: an R package to fit regression models with broken-line relationships. *R. News* 8 (1), 20–25.
- National Ecological Observatory Network, 2020. Data product DP1.10055.001. Plant Phenology Observations.
- National Ecological Observatory Network, 2023. NEON Geolocation Repository [R]. National Ecological Observatory Network. <https://github.com/NEONScience/NEON-geolocation>.
- Pearse, W.D., Davis, C.C., Inouye, D.W., Primack, R.B., Davies, T.J., 2017. A statistical estimator for determining the limits of contemporary and historic phenology. *Nature Ecology & Evolution* 1 (12), 12. <https://doi.org/10.1038/s41559-017-0350-0>.
- Planet Team, 2017. Planet application program interface: in space for life on Earth. <http://api.planet.com>.
- Planet Team, 2023. Udm 2. <https://developers.planet.com/docs/data/udm-2/>.
- Polgar, C.A., Primack, R.B., 2011. Leaf-out phenology of temperate woody plants: from trees to ecosystems. *New Phytol.* 191 (4), 926–941. <https://doi.org/10.1111/j.1469-8137.2011.03803.x>.
- Portnoy, J., Barnes, C., Barnes, C.S., 2004. The national allergy Bureau: pollen and spore reporting today. *J. Allergy Clin. Immunol.* 114 (5), 1235–1238. <https://doi.org/10.1016/j.jaci.2004.07.062>.
- Post, E., 2013. Ecology of climate change: the importance of biotic interactions. In: *Ecology of Climate Change*. Princeton University Press. <https://doi.org/10.1515/9781400846139>.
- Primack, R.B., 1985. Patterns of flowering phenology in communities, populations, individuals, and single flowers. In: White, J. (Ed.), *The Population Structure of Vegetation*. Springer, Netherlands, pp. 571–593. [https://doi.org/10.1007/978-94-009-5500-4\\_24](https://doi.org/10.1007/978-94-009-5500-4_24).
- Psutka, J.V., Psutka, J., 2019. Sample size for maximum-likelihood estimates of Gaussian model depending on dimensionality of pattern space. *Pattern Recogn.* 91, 25–33. <https://doi.org/10.1016/j.patcog.2019.01.046>.
- R Core Team, 2024. R: A Language and Environment for Statistical Computing. R Foundation for Statistical Computing, Vienna, Austria. <https://www.r-project.org/>.
- Reid, C.E., Gamble, J.L., 2009. Aeroallergens, allergic disease, and climate change: impacts and adaptation. *EcoHealth* 6 (3), 458–470. <https://doi.org/10.1007/s10393-009-0261-x>.
- Robichaud, A., Comtois, P., 2021. Numerical modelling of birch pollen dispersion in Canada. *Environ. Res.* 194, 110554. <https://doi.org/10.1016/j.envres.2020.110554>.
- Rojo, J., Romero-Morte, J., Lara, B., Quirós, E., Richardson, A.D., Pérez-Badia, R., 2022. Biological-based and remote sensing techniques to link vegetative and reproductive development and assess pollen emission in Mediterranean grasses. *Ecol. Inform.* 72, 101898. <https://doi.org/10.1016/j.ecoinf.2022.101898>.
- Rosemartin, A.H., Denny, E.G., Gerst, K.L., Marsh, R.L., Posthumus, E.E., Crimmins, T.M., Weltzin, J.F., 2018. USA. National Phenology Network Observational Data Documentation (USGS Numbered Series 2018–1060; Open-File Report, P. 30). U.S. Geological Survey. <http://pubs.er.usgs.gov/publication/ofr20181060>.
- Scheifinger, H., Belmonte, J., Butters, J., Celenk, S., Damialis, A., Dechamp, C., García-Mozo, H., Gehrig, R., Grewling, L., Halley, J.M., Hogda, K.-A., Jäger, S., Karatzas, K., Karlsen, S.-R., Koch, E., Pauling, A., Peel, R., Sikoparija, B., Smith, M., et al., 2013. Monitoring, modelling and forecasting of the pollen season. In: Sofiev, M., Bergmann, K.-C. (Eds.), *Allergenic Pollen: A Review of the Production, Release, Distribution and Health Impacts*. Springer Netherlands, pp. 71–126. [https://doi.org/10.1007/978-94-007-4881-1\\_4](https://doi.org/10.1007/978-94-007-4881-1_4).
- Seo, Y.A., Kim, K.R., Cho, C., Oh, J.-W., Kim, T.H., 2019. Deep neural network-based concentration model for oak pollen allergy warning in South Korea. *Allergy, Asthma & Immunology Research* 12 (1), 149–163. <https://doi.org/10.4168/airr.2020.12.1.149>.
- Singh, A.B., Kumar, P., 2022. Climate change and allergic diseases: an overview. *Frontiers in Allergy* 3. <https://doi.org/10.3389/falgy.2022.964987>.
- Singh, D., Singh, B., 2020. Investigating the impact of data normalization on classification performance. *Appl. Soft Comput.* 97, 105524. <https://doi.org/10.1016/j.asoc.2019.105524>.
- Sofiev, M., Berger, U., Prank, M., Vira, J., Arteta, J., Belmonte, J., Bergmann, K.-C., Chéroux, F., Elbern, H., Friese, E., Galan, C., Gehrig, R., Khorostyanov, D., Kranenburg, R., Kumar, U., Marécal, V., Meleux, F., Menut, L., Pessi, A.-M., et al., 2015. MACC regional multi-model ensemble simulations of birch pollen dispersion in Europe. <https://doi.org/10.5194/acpd-15-8243-2015>.
- Sofiev, M., Palamarchuk, J., Kouznetsov, R., Abramidze, T., Adams-Groom, B., Antunes, C.M., Ariño, A.H., Basti, M., Belmonte, J., Berger, U.E., Bonini, M., Bruffaerts, N., Butters, J., Cariñanos, P., Celenk, S., Ceriotti, V., Charalampopoulos, A., Clewlow, Y., Clot, B., et al., 2024. European pollen reanalysis, 1980–2022, for alder, birch, and olive. *Sci. Data* 11 (1), 1082. <https://doi.org/10.1038/s41597-024-03686-2>.
- Sofiev, M., Siljamo, P., Ranta, H., Rantio-Lehtimäki, A., 2006. Towards numerical forecasting of long-range air transport of birch pollen: theoretical considerations and a feasibility study. *Int. J. Biometeorol.* 50 (6), 392–402. <https://doi.org/10.1007/s00484-006-0027-x>.
- Song, Y., Munch, S.B., Zhu, K., 2023. Prediction-based approach for quantifying phenological mismatch across landscapes under climate change. *Landsc. Ecol.* 38 (3), 821–845. <https://doi.org/10.1007/s10980-023-01595-0>.
- Suanno, C., Aloisi, I., Fernández-González, D., Del Duca, S., 2021. Pollen forecasting and its relevance in pollen allergen avoidance. *Environ. Res.* 200, 111150. <https://doi.org/10.1016/j.envres.2021.111150>.
- Taylor, S.D., White, E.P., 2020. Automated data-intensive forecasting of plant phenology throughout the United States. *Ecol. Appl.* 30 (1), e02025. <https://doi.org/10.1002/ep.2025>.
- Templ, B., Koch, E., Bolmgren, K., Ungersböck, M., Paul, A., Scheifinger, H., Rutishauser, T., Bustos, M., Chmielewski, F.-M., Hájková, L., Hodžíč, S., Kaspar, F., Pietragalla, B., Romero-Fresneda, R., Tolvanen, A., Vučetić, V., Zimmermann, K., Züst, A., 2018. Pan-European Phenological database (PEP725): a single point of access for European data. *Int. J. Biometeorol.* 62 (6), 1109–1113. <https://doi.org/10.1007/s00484-018-1512-8>.
- Verstraeten, W.W., Kouznetsov, R., Bruffaerts, N., Sofiev, M., Delcloo, A.W., 2024. Assessing uncertainty in airborne birch pollen modelling. *Aerobiologia* 40 (2), 271–286. <https://doi.org/10.1007/s10453-024-09818-w>.
- Verstraeten, W.W., Kouznetsov, R., Hoebcke, L., Bruffaerts, N., Sofiev, M., Delcloo, A.W., 2022. Reconstructing multi-decadal airborne birch pollen levels based on NDVI data and a pollen transport model. *Agric. For. Meteorol.* 320, 108942. <https://doi.org/10.1016/j.agrformet.2022.108942>.
- Vitassee, Y., Baumgarten, F., Zohner, C.M., Kaewthongrach, R., Fu, Y.H., Walde, M.G., Moser, B., 2021. Impact of microclimatic conditions and resource availability on spring and autumn phenology of temperate tree seedlings. *New Phytol.* 232 (2), 537–550. <https://doi.org/10.1111/nph.17606>.

- Vogel, H., Pauling, A., Vogel, B., 2008. Numerical simulation of birch pollen dispersion with an operational weather forecast system. *Int. J. Biometeorol.* 52 (8), 805–814. <https://doi.org/10.1007/s00484-008-0174-3>.
- Wang, H., Wang, H., Ge, Q., Dai, J., 2020. The interactive effects of chilling, photoperiod, and forcing temperature on flowering phenology of temperate woody plants. *Front. Plant Sci.* 11. <https://doi.org/10.3389/fpls.2020.00443>.
- Weinberger, K.R., Kinney, P.L., Robinson, G.S., Sheehan, D., Kheirbek, I., Matte, T.D., Lovasi, G.S., 2018. Levels and determinants of tree pollen in New York City. *J. Expo. Sci. Environ. Epidemiol.* 28 (2), 2. <https://doi.org/10.1038/jes.2016.72>.
- Weinstein, B.G., Graves, S.J., Marconi, S., Singh, A., Zare, A., Stewart, D., Bohlman, S.A., White, E.P., 2021. A benchmark dataset for canopy crown detection and delineation in co-registered airborne RGB, LiDAR and hyperspectral imagery from the National Ecological Observation Network. *PLoS Comput. Biol.* 17 (7), e1009180. <https://doi.org/10.1371/journal.pcbi.1009180>.
- Wozniak, M.C., Steiner, A.L., 2017. A prognostic pollen emissions model for climate models (PECM1.0). *Geosci. Model Dev. (GMD)* 10 (11), 4105–4127. <https://doi.org/10.5194/gmd-10-4105-2017>.
- Wu, S., Wang, J., Yan, Z., Song, G., Chen, Y., Ma, Q., Deng, M., Wu, Y., Zhao, Y., Guo, Z., Yuan, Z., Dai, G., Xu, X., Yang, X., Su, Y., Liu, L., Wu, J., 2021. Monitoring tree-crown scale autumn leaf phenology in a temperate forest with an integration of PlanetScope and drone remote sensing observations. *ISPRS J. Photogrammetry Remote Sens.* 171, 36–48. <https://doi.org/10.1016/j.isprsjprs.2020.10.017>.
- Yang, X., Zhu, W., Zhao, C., 2022. A prediction model for the outbreak date of spring pollen allergy in Beijing based on satellite-derived phenological characteristics of vegetation greenness. *Remote Sens.* 14 (22), 22. <https://doi.org/10.3390/rs14225891>.
- Zapata-Marin, S., Schmidt, A.M., Weichenthal, S., Katz, D.S.W., Takaro, T., Brook, J., Lavigne, E., 2022. Within city spatiotemporal variation of pollen concentration in the city of Toronto, Canada. *Environ. Res.* 206, 112566. <https://doi.org/10.1016/j.envres.2021.112566>.
- Zewdie, G.K., Lary, D.J., Levetin, E., Garuma, G.F., 2019. Applying deep neural networks and ensemble machine learning methods to forecast airborne Ambrosia pollen. *Int. J. Environ. Res. Publ. Health* 16 (11), 11. <https://doi.org/10.3390/ijerph16111992>.
- Zhang, Y., Steiner, A.L., 2022. Projected climate-driven changes in pollen emission season length and magnitude over the continental United States. *Nat. Commun.* 13 (1), 1. <https://doi.org/10.1038/s41467-022-28764-0>.
- Zhao, Y., Lee, C.K.F., Wang, Z., Wang, J., Gu, Y., Xie, J., Law, Y.K., Song, G., Bonebrake, T.C., Yang, X., Nelson, B.W., Wu, J., 2022. Evaluating fine-scale phenology from PlanetScope satellites with ground observations across temperate forests in eastern North America. *Rem. Sens. Environ.* 283, 113310. <https://doi.org/10.1016/j.rse.2022.113310>.
- Zhu, X., Ma, X., Zhang, Z., Liu, Y., Luo, Y., Yan, K., Pei, T., Huete, A., 2024. Floating in the air: forecasting allergenic pollen concentration for managing urban public health. *International Journal of Digital Earth* 17 (1), 2306894. <https://doi.org/10.1080/17538947.2024.2306894>.
- Ziska, L.H., Caulfield, F.A., 2000. Rising CO<sub>2</sub> and pollen production of common ragweed (*Ambrosia artemisiifolia* L.), a known allergy-inducing species: implications for public health. *Funct. Plant Biol.* 27 (10), 893–898. <https://doi.org/10.1071/pp00032>.
- Ziska, L.H., Knowlton, K., Rogers, C., Dalan, D., Tierney, N., Elder, M.A., Filley, W., Shropshire, J., Ford, L.B., Hedberg, C., Fleetwood, P., Hovanky, K.T., Kavanagh, T., Fulford, G., Vrtis, R.F., Patz, J.A., Portnoy, J., Coates, F., Bielory, L., Frenz, D., 2011. Recent warming by latitude associated with increased length of ragweed pollen season in central North America. *Proc. Natl. Acad. Sci. USA* 108 (10), 4248–4251. <https://doi.org/10.1073/pnas.1014107108>.
- Ziska, L.H., Makra, L., Harry, S.K., Bruffaerts, N., Hendrickx, M., Coates, F., Saarto, A., Thibaudeau, M., Oliver, G., Damialis, A., Charalampopoulos, A., Vokou, D., Heidmarsson, S., Gutjohnsen, E., Bonini, M., Oh, J.-W., Sullivan, K., Ford, L., Brooks, G.D., et al., 2019. Temperature-related changes in airborne allergenic pollen abundance and seasonality across the northern hemisphere: a retrospective data analysis. *Lancet Planet. Health* 3 (3), e124–e131. [https://doi.org/10.1016/S2542-5196\(19\)30015-4](https://doi.org/10.1016/S2542-5196(19)30015-4).